

Permutation in the CHY-Formulation

Rijun Huang,^a Fei Teng^{1b} and Bo Feng^{2c,d}

^a*Institute of Theoretical Physics, School of Physics and Technology, Nanjing Normal University,
No.1 Wenyuan Road, Nanjing 210023, P. R. China.*

^b*Department of Physics and Astronomy, Uppsala University,
Box 516, SE-751 20 Uppsala, Sweden.*

^c*Zhejiang Institute of Modern Physics, Department of Physics, Zhejiang University,
No.38 Zheda Road, Hangzhou 310027, P.R. China.*

^d*Center of Mathematical Science, Zhejiang University,
No.38 Zheda Road, Hangzhou 310027, P.R. China.*

E-mail: huang@nbi.dk, fei.teng@physics.uu.se, fengbo@zju.edu.cn

ABSTRACT: The CHY-integrand of bi-adjoint cubic scalar theory is a product of two PT-factors. This pair of PT-factors can be interpreted as defining a permutation. We introduced the cycle representation of permutation in this paper for the understanding of cubic scalar amplitude. We showed that, given a permutation related to the pair of PT-factors, the pole and vertex information of Feynman diagrams of corresponding CHY-integrand is completely characterized by the cycle representation of permutation. Inversely, we also showed that, given a set of Feynman diagrams, the cycle representation of corresponding PT-factor can be recursively constructed. Based on these results, we have investigated the relations among different independent pairs of PT-factors in the context of cycle representation as well as the multiplication of cross-ratio factors.

KEYWORDS: CHY-formulation, Permutation, Amplitude

¹The corresponding author.

²The unusual ordering of authors instead of the standard alphabet ordering is for young researchers to get proper recognition of contributions under the current out-dated practice in China.

Contents

1	Introduction	1
2	The setup	3
2.1	The canonical PT-factor	3
2.2	Permutation, cycle representation and PT-factor	4
3	From permutations to Feynman diagrams	5
3.1	The three and four point cases	10
3.2	The five point case	11
3.3	The six point case	13
3.4	Higher point examples	20
4	From Feynman diagrams to permutations	23
4.1	The zig-zag path and cycle-representation of permutation	25
4.2	The recursive construction of PT-factor via cycle representation	28
4.3	Examples	31
5	Relations between different PT-factors	32
5.1	Relation analysis via cycle representation	33
5.2	Relation analysis via cross-ratio factor	37
6	Conclusion	43
A	Associahedron and cycle representation of permutation	44

1 Introduction

It was first proposed by Cachazo, He and Yuan (CHY) [1–4] that the tree-level scattering amplitudes of many massless theories are supported by the solutions to the scattering equations

$$f_i = \sum_{j=1, j \neq i}^n \frac{s_{ij}}{\sigma_{ij}} = 0, \quad i = 1, 2 \dots n, \quad (1.1)$$

where $s_{ij} = (p_i + p_j)^2$ are Mandelstam variables, and $\sigma_{ij} = \sigma_i - \sigma_j$ are moduli space variables. The CHY-formulation consists of an integrand \mathcal{I}_n that specifies the theory, and a measure on the moduli space that

fully localizes the integration to the solutions of the scattering equations (1.1):

$$\int d\mu_{\text{CHY}} = \int (\sigma_{rs}\sigma_{st}\sigma_{tr})^2 \prod_{i \neq r,s,t} d\sigma_i \delta(f_i) . \quad (1.2)$$

The moduli space integration indicates that the CHY-formulation should appear as a certain limit of the string amplitudes, which effectively reduces the path ordered string measure into the color ordered CHY measure. It has been shown that the CHY-formulation naturally emerges as the infinite tension limit of ambitwistor strings [5–7], chiral strings [8, 9] and pure spinor formalism of superstrings [10, 11]. In the context of conventional string theory, the CHY-formulation can also appear as the zero tension limit of an alternative dual model [12].

The scattering equations (1.1) have $(n - 3)!$ solutions, and to obtain the amplitudes, naively one needs to get all the solutions and sum up their contributions. However, solving the equations becomes computationally unavailable as the number of particles grows. This difficulty can be circumvented by using integration rules [13–16]. The idea behind this approach is that one can obtain the sum over algebraic combinations of the solutions in terms of the coefficients of the original polynomial equations without knowing each individual solution. Using the original integration rules, we can extract the correct amplitudes of those theories without the appearance of higher order poles, for example, the bi-adjoint scalar theory whose integrand consists of two Parke-Taylor (PT) factors,

$$\begin{aligned} \mathcal{I}_n &= \text{PT}(\boldsymbol{\alpha}) \times \text{PT}(\boldsymbol{\beta}) = \langle \alpha_1 \alpha_2 \cdots \alpha_n \rangle \times \langle \beta_1 \beta_2 \cdots \beta_n \rangle \\ &= \frac{1}{\sigma_{\alpha_1 \alpha_2} \sigma_{\alpha_2 \alpha_3} \cdots \sigma_{\alpha_n \alpha_1}} \times \frac{1}{\sigma_{\beta_1 \beta_2} \sigma_{\beta_2 \beta_3} \cdots \sigma_{\beta_n \beta_1}} , \end{aligned} \quad (1.3)$$

where $\boldsymbol{\alpha} = \{\alpha_1, \dots, \alpha_n\}$ and $\boldsymbol{\beta} = \{\beta_1, \dots, \beta_n\}$ are two permutations of external particles. On the other hand, theories with more complicated integrands usually involve (spurious) higher order poles. For example, by expanding the Yang-Mills integrand following the way of Lam and Yao [17], one has to develop various techniques to evaluate the higher order poles and show that they indeed cancel towards the end [18–22]. Alternatively, one can expand the integrand in terms of linear combinations of bi-adjoint scalar ones with local coefficients, such that the calculation of higher order poles can be avoided. This approach has succeeded in Yang-Mills, Yang-Mills-scalar and nonlinear sigma model [23–28]. The latter approach has an extra benefit that the expansion coefficients are automatically the Bern-Carrasco-Johansson numerators [4, 29, 30]. It is not surprising that the amplitudes of various theories land on the bi-adjoint scalar ones after a recursive expansion. The reason is that these bi-adjoint scalar amplitudes capture exactly the physical poles associated with various diagrams that are planar under certain color ordering, while different theories just dress these diagrams with different kinematic numerators.

The above discussion shows the fundamental role of the bi-adjoint cubic scalar amplitudes in the understanding of CHY-formulation, so it is not surprising that many different approaches have been proposed towards the evaluation and better understanding of CHY-integrand with product of two PT-factors. While many of them focus on the rational function of complex variables σ_i 's, in paper [31] the authors have related the PT-factors to the partial triangulations of a polygon with n edges (n -gon), and the PT-factors are

deeply connected to the associahedron. It also brings permutation group S_n into the story, since each PT-factor is accompanied by a color trace with a definite ordering. We should find one-to-one correspondence between action of S_n onto the PT-factors and partial triangulations of n -gon. It would be a very natural idea to understand the CHY-integrand from the knowledge of permutations. Certain progress along this direction has been made in [32] by investigating pairing of external legs, whose results are presented in terms of illustrative objects like *crystal* and *defect*. In fact, for the two PT-factors in the CHY-integrand of bi-adjoint cubic scalar theory, if we set one PT-factor as the natural ordering $\langle 12 \cdots n \rangle$, corresponding to identity element in the permutation group, then the other PT-factor can be interpreted as a permutation acting on the identity. The physical information, i.e., the poles and vertices of the Feynman diagrams that this CHY-integrand evaluates to, should find its clue in the structure of permutations. In this paper, we try to understand the cubic scalar amplitude by inspecting the structure of permutations. We demonstrate how the physical information is encoded in the permutations, and explore the relations of different PT-factors from the means of permutations as well as other algebraic methods stemmed from the integration rules.

This paper is organized as follows. In §2, we set our convention and provide some necessary backgrounds. In §3, we show how the structure of those Feynman diagrams produced by a CHY-integrand can be extracted from the cycle representations of the corresponding PT-factor viewed as a permutation. In §4, we study the inverse problem on how to write out the PT-factor for an arbitrary given Feynman diagram. In the form of cycle representation, we propose a recursive method to construct an n -point PT-factor recursively from lower point PT-factors. In §5, we investigate the relations among different PT-factors via the merging and splitting of cycle representations, as well as via multiplying cross-ratio factors. Conclusion is presented in §6, and in Appendix A, we comment on an interesting interplay between the associahedron and cycle representations of permutation.

2 The setup

In this section, we give the definitions of some important objects to be used in later.

2.1 The canonical PT-factor

Since the $2n$ PT-factors obtained by acting cyclic rotations and reflections evaluate to the same amplitude, despite an overall sign $(-1)^n$ for the latter case, all these $2n$ PT-factors form an *equivalent class*. Thus the number of independent PT-factors is $n!/(2n)$. We can represent each independent PT-factors by a *canonical* ordering $\langle \alpha_1 \alpha_2 \cdots \alpha_n \rangle$ that satisfy two conditions: (1) the first element α_1 is fixed to be 1 to eliminate the cyclic ambiguity, (2) the second element α_2 should be smaller than the last element α_n to eliminate the reversing ambiguity. The complete equivalent class can be generated from these independent PT-factors by acting the cyclic rotation and reversing. For example, up to $n = 5$, we can choose the independent

PT-factors as follows,

$$\begin{aligned}
n = 3 \quad \# = \frac{n!}{2n} = 1 : \quad & \langle 123 \rangle , \\
n = 4 \quad \# = \frac{n!}{2n} = 3 : \quad & \langle 1234 \rangle , \quad \langle 1243 \rangle , \quad \langle 1324 \rangle , \\
n = 5 \quad \# = \frac{n!}{2n} = 12 : \quad & \langle 12345 \rangle , \quad \langle 12354 \rangle , \quad \langle 12435 \rangle , \quad \langle 12453 \rangle , \quad \langle 12534 \rangle , \quad \langle 12543 \rangle , \\
& \langle 13245 \rangle , \quad \langle 13254 \rangle , \quad \langle 13425 \rangle , \quad \langle 13524 \rangle , \quad \langle 14235 \rangle , \quad \langle 14325 \rangle .
\end{aligned}$$

The CHY-integrand for bi-adjoint cubic scalar amplitudes is given by $\text{PT}(\boldsymbol{\alpha}) \times \text{PT}(\boldsymbol{\beta})$, as shown in Eq. (1.3). A simultaneous permutation acting on $\boldsymbol{\alpha}$ and $\boldsymbol{\beta}$ merely leads to the same result up to a relabeling of external legs. Hence we can fix one of the PT-factors to be the natural ordering $\text{PT}(\boldsymbol{\alpha}) = \langle 12 \cdots (n-1)n \rangle$, and consider the other PT-factor $\text{PT}(\boldsymbol{\beta})$ as a permutation acting on $\boldsymbol{\alpha}$. Thus all the dynamical information is encoded in $\text{PT}(\boldsymbol{\beta})$, from which one can read out the amplitude.

2.2 Permutation, cycle representation and PT-factor

Permutations, as group elements of the n -point symmetric group S_n , can be defined by their action onto the space spanned by the elements of S_n themselves, for example,

$$\boldsymbol{\beta}|e\rangle = |\boldsymbol{\beta}\rangle \quad , \quad \boldsymbol{\gamma}\boldsymbol{\beta}|e\rangle = \boldsymbol{\gamma}|\boldsymbol{\beta}\rangle = |\boldsymbol{\gamma}\boldsymbol{\beta}\rangle \quad , \quad (2.1)$$

where $\boldsymbol{\beta}$ and $\boldsymbol{\gamma}$ are two generic elements of S_n , and e is the identity element defined as the natural ordering $\{1, 2, \dots, n\}$. Each permutation can be represented by a product of disjoint cycles $(i_1 i_2 \cdots i_s)$, which stands for the map $i_1 \mapsto i_2, i_2 \mapsto i_3, \dots, i_s \mapsto i_1$. For example,

$$(123)(4)(5) \cdots (n) |1234 \cdots n\rangle = |2314 \cdots n\rangle \quad (2.2)$$

stands for the permutation in Cauchy's two-line notation

$$\begin{pmatrix} 1 & 2 & 3 & 4 & \cdots & n \\ 2 & 3 & 1 & 4 & \cdots & n \end{pmatrix} . \quad (2.3)$$

Cycles are defined up to a cyclic ordering, for example, $(123) = (231) = (312)$ gives the same permutation. It is also obvious that two disjoint cycles commute, i.e., $(123)(45) = (45)(123)$. Each permutation has a unique decomposition in terms of disjoint cycles, modulo the cyclicity of each cycle and the ordering of disjoint cycles.¹ We call this unique decomposition the *cycle representation* of a permutation in the rest of this paper. The number of disjoint cycles in a cycle representation is called the length of this cycle representation, and the number of elements in a cycle is called the length of cycle.

¹In this statement, *disjoint* is crucial to the uniqueness. Otherwise, we could have other decompositions like $(1)(2) = (12)(12)$, etc.

In our CHY-integrand (1.3), we can treat $\text{PT}(\boldsymbol{\beta}) = \langle \beta_1 \beta_2 \cdots \beta_n \rangle$ also as a permutation. The equivalent class of $\text{PT}(\boldsymbol{\beta})$ consists of all the $2n$ permutations obtained by cyclic rotations and reversing,

$$\mathfrak{b}[\boldsymbol{\beta}] := \left\{ \begin{array}{l} \langle \beta_1 \beta_2 \cdots \beta_{n-1} \beta_n \rangle, \langle \beta_2 \beta_3 \cdots \beta_n \beta_1 \rangle, \dots, \langle \beta_n \beta_1 \cdots \beta_{n-2} \beta_{n-1} \rangle \\ \langle \beta_n \beta_{n-1} \cdots \beta_2 \beta_1 \rangle, \langle \beta_1 \beta_n \cdots \beta_3 \beta_2 \rangle, \dots, \langle \beta_{n-1} \beta_{n-2} \cdots \beta_1 \beta_n \rangle \end{array} \right\}. \quad (2.4)$$

We define the cyclic generator \mathbf{g}_c and reversing generator \mathbf{g}_r respectively as

$$\mathbf{g}_c = (\beta_1 \beta_2 \cdots \beta_n) \quad , \quad \mathbf{g}_r = \begin{cases} (\beta_1 \beta_n)(\beta_2 \beta_{n-1}) \cdots (\beta_{\frac{n}{2}} \beta_{\frac{n+2}{2}}) & \text{for even } n \\ (\beta_1 \beta_n)(\beta_2 \beta_{n-1}) \cdots (\beta_{\frac{n-1}{2}} \beta_{\frac{n+3}{2}})(\beta_{\frac{n+1}{2}}) & \text{for odd } n \end{cases}, \quad (2.5)$$

which satisfy the relation $\mathbf{g}_r \mathbf{g}_c = \mathbf{g}_c^{-1} \mathbf{g}_r$ and $\mathbf{g}_c^n = \mathbf{g}_r^2 = \mathbf{e}$. Thus they generate the n -point dihedral group D_n . For a permutation $\boldsymbol{\beta}$, the equivalent class $\mathfrak{b}[\boldsymbol{\beta}]$ is thus given by,

$$\mathfrak{b}[\boldsymbol{\beta}] = \{ \boldsymbol{\beta}, \boldsymbol{\beta} \mathbf{g}_c, \dots, \boldsymbol{\beta} \mathbf{g}_c^{n-1}, \boldsymbol{\beta} \mathbf{g}_r, \boldsymbol{\beta} \mathbf{g}_r \mathbf{g}_c, \dots, \boldsymbol{\beta} \mathbf{g}_r \mathbf{g}_c^{n-1} \}. \quad (2.6)$$

The elements in \mathfrak{b} has one-to-one correspondence to the equivalent class of PT-factors (2.4). There are in all $n!/(2n)$ non-equivalent permutations. However, they do not form a group in general, since D_n is not a normal subgroup of S_n for $n \geq 4$. For permutations in the same equivalent class, of course they have different cycle representations, since after all they are different group elements of S_n . In the next section, we are going to show that which set of Feynman diagrams $\text{PT}(\boldsymbol{\beta})$ corresponds to is encoded collectively in the different cycle representations of the equivalent permutations in \mathfrak{b} .

3 From permutations to Feynman diagrams

One of our motivations is to explore the information encoded in the PT-factors, described in the form of permutations. As mentioned in the previous section, in our setup the amplitude result is determined by the second PT-factor $\text{PT}(\boldsymbol{\beta})$, considered to be a permutation acting on the identity element. It determines an equivalent class containing $2n$ elements evaluating to the same amplitude. Thus we need to consider all the permutations in the equivalent class. For example, when working with the CHY-integrand $\text{PT}(\boldsymbol{\alpha}) \times \text{PT}(\boldsymbol{\beta}) = \langle 1234 \rangle \times \langle 1243 \rangle$, we need the equivalent class of $\langle 1243 \rangle$, containing eight elements,

$$\left\{ \langle 1243 \rangle, \langle 2431 \rangle, \langle 4312 \rangle, \langle 3124 \rangle, \langle 3421 \rangle, \langle 4213 \rangle, \langle 2134 \rangle, \langle 1342 \rangle \right\}, \quad (3.1)$$

or in the form of cycle representations,

$$\left\{ (1)(2)(34), (124)(3), (1423), (132)(4), (1324), (143)(2), (12)(3)(4), (1)(234) \right\}. \quad (3.2)$$

Our purpose is to relate these cycle representations to the Feynman diagrams contributing to the amplitude. All the above eight cycle representations in (3.2) can be used to reconstruct the PT-factor $\text{PT}(\boldsymbol{\beta})$ by acting them on the natural ordering $\langle 1234 \rangle$, so each one encodes the complete information for evaluation. However, they have different structures. In Eq. (3.2), two cycle representations are length-1, four are length-2, while the remaining two are length-3. How can we read useful information out of these different cycle structures?

To answer this question, let us recall the integral result of the CHY-integrand $\langle 1234 \rangle \times \langle 1243 \rangle$, which is $-\frac{1}{s_{12}}$. It corresponds to a Feynman diagram with two cubic vertices, one connecting the legs 1, 2 and the internal propagator $P_{12} := p_1 + p_2$, while the other connecting the legs 3, 4, and the internal propagator $-P_{12}$. It is very plausible to conjecture that, the two cycle representations (1)(2)(34) and (12)(3)(4) in fact describe respectively the two cubic vertices. In (1)(2)(34), the two cycles (1) and (2) describe respectively the external legs 1 and 2 attached to a vertex, while the cycle (34) describes the corresponding internal propagator of that vertex. It also indicates that $\frac{1}{s_{34}} = \frac{1}{s_{12}}$ is an internal pole. Similar analysis can be carried out for the cycle representation (12)(3)(4).

Above discussion tells us that, although each cycle representation contains the complete information of amplitude, the pole structure is manifest in some of them but not all. The complete picture of Feynman diagrams is determined collectively by all cycle representations whose pole and/or vertex structures are manifest. With this understanding, we only need to consider those good cycle representations, i.e., the pole and/or vertex structure are manifest. For bi-scalar theory, the physical pole would appear only for the external legs with consecutive ordering. So let us define the *good cycle representations* as those satisfying the following criteria:

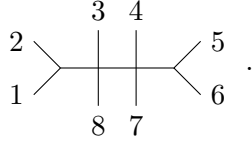
- the cycles in the considered cycle representation can be separated into at least two parts, while the union of cycles in each part is consecutive (later called *planar separation*).
- in case that the cycle representation *can only be* separated into two parts, then each part should contain at least two elements.

Moreover, if the planar separation of a good cycle representation contains at least three parts, we call it a *vertex type* (V-type) cycle representation. Otherwise, we call it a *pole type* (P-type) cycle representation. Let us give a few more examples. At six point, both (12)(34)(56) and (12)(35)(46) are good cycle representations. The former is a V-type one since it can be separated into three parts (12), (34) and (56), while the latter is a P-type one since it can only be separated into two parts (12) and (35)(46). On the other hand, both (14)(25)(36) and (1)(23456) are bad cycle representations according to the above criteria, since the former one has no planar separation at all while the separated part (1) in the latter contains only one element. With the above definitions, we can give an answer to the question raised at the end of the first paragraph of this section: we can reconstruct the Feynman diagrams by considering all the good cycle representations in the equivalent class of a PT-factor.

Now we illustrate how a good cycle representation reflects the vertex and pole structure of the corresponding Feynman diagram by an eight point example $\text{PT}(\boldsymbol{\beta}) = \langle 12846573 \rangle$, which gives four trivalent Feynman diagrams after the CHY integration,

$$\frac{1}{s_{12}s_{56}s_{8123}} \left(\frac{1}{s_{812}} + \frac{1}{s_{123}} \right) \left(\frac{1}{s_{456}} + \frac{1}{s_{567}} \right). \quad (3.3)$$

The result can be summarized into a single effective Feynman diagram,



There are 16 equivalent cycle representations in $\mathfrak{b}[\beta]$, collected as,

$$\begin{aligned}
 \text{good :} \quad & \text{V-type :} \quad (1)(2)(38)(4)(56)(7) \quad , \quad (12)(3)(47)(5)(6)(8) \quad , \\
 & \text{P-type :} \quad (132)(4875)(6) \quad , \quad (128)(3467)(5) \quad , \quad (1)(2378)(456) \quad , \quad (1843)(2)(576) \quad , \\
 \text{bad :} \quad & (15274)(3)(68) \quad , \quad (14726)(35)(8) \quad , \quad (16385)(24)(7) \quad , \quad (17)(25836)(4) \quad , \\
 & (176423)(58) \quad , \quad (182457)(36) \quad , \quad (135468)(27) \quad , \quad (14)(286753) \quad , \\
 & (1526)(3487) \quad , \quad (1625)(3784) \quad .
 \end{aligned} \tag{3.4}$$

In general, P-type cycle representations manifest certain poles contained in some of the Feynman diagrams. For example, $(132)|(4875)(6)$ is P-type since it can only be divided into two parts indicated by the vertical line. This separation indicates that the pole s_{123} should appear in some Feynman diagrams. Similarly, the other three P-type cycle representations correspond respectively to the pole s_{812} , s_{456} and s_{567} , as can be seen in Eq. (3.3). In contrary, the V-type cycle representations contain both pole and vertex information. For example, the cycle representation $(1)(2)(38)(4)(56)(7)$ allows two different planar separations,

$$\text{four parts :} \quad (1)(2)(38)|(4)|(56)|(7) \quad , \tag{3.5a}$$

$$\text{three parts :} \quad (1)|(2)|(38)(4)(56)(7) \quad . \tag{3.5b}$$

These two separations indicate that the effective Feynman diagram contains one quartic vertex with legs $\{P_{8123}, 4, P_{56}, 7\}$, and one cubic vertex with legs $\{1, 2, P_{345678}\}$. Since the legs with more than one elements also give pole information, we can read out the poles s_{8123} , s_{56} , and s_{12} from this V-type cycle representation. Similarly, the cycle representation $(12)(3)(47)(5)(6)(8)$ gives one quartic vertex with legs $\{P_{12}, 3, P_{4567}, 8\}$ and one cubic vertex with legs $\{5, 6, P_{781234}\}$, and it gives the same pole structures as the previous one. Combining these two, we do produce all the vertices in the effective Feynman diagram.

The above example shows that by collectively combining the information from all good cycle representations, we can read out the complete Feynman diagram result. This provides one method of analysis. On the other hand, we can arrive at the complete final result by relying on only one good cycle representation, since each one should contain the complete information of PT-factor $\text{PT}(\beta)$. Hence we should have another method of analysis. Observations from practical computation show that,

- (A) All V-type cycle representations together manifest the vertex structure of the corresponding effective Feynman diagram.

- (B) It is also possible to reproduce the effective Feynman diagram from one V-type cycle representation if we recursively use the lower multiplicity results.
- (C) One P-type cycle representation is not sufficient to reproduce the complete result, and in order to get the correct answer we should consider all P-type cycle representations.

We use again the example (3.4) to demonstrate our observations. We start with the V-type cycle representation (1)(2)(38)(4)(56)(7). In the four-part separation (3.5a), we first coarse grain the part {8123} and {56} by replacing them by a single propagator. This leads to an effective quartic vertex,

$$\begin{aligned} \text{PT}(\boldsymbol{\beta}) &= (1)(2)(38)|(4)|(56)|(7) \rightarrow (P_{8123})(4)(P_{56})(7) , \\ \text{PT}(\boldsymbol{\alpha}) &= (8)(1)(2)(3)|(4)|(5)(6)|(7) \rightarrow (P_{8123})(4)(P_{56})(7) , \end{aligned}$$

which gives the contribution

$$P_{8123} \begin{array}{c} 4 \\ \diagdown \\ \diagup \\ 7 \end{array} P_{56} = \frac{1}{s_{8123}s_{56}} \left(\frac{1}{s_{4P_{56}}} + \frac{1}{s_{P_{56}7}} \right) = \frac{1}{s_{8123}s_{56}} \left(\frac{1}{s_{456}} + \frac{1}{s_{567}} \right) . \quad (3.6)$$

Next, we look into the substructures. In Eq. (3.5a), the substructure $\{P_{56}, 5, 6\}$ has the cycle representation $(P_{56})(56)$. In its equivalent class, we have only one good cycle representation

$$\text{V-type : } (P_{56})(5)(6) \implies P_{56} \begin{array}{c} 5 \\ \diagdown \\ \diagup \\ 6 \end{array} , \quad (3.7)$$

which gives the familiar cubic vertex. The substructure $\{P_{8123}, 8, 1, 2, 3\}$ has the cycle representation (1)(2)(38)(P_{8123}) in Eq. (3.5a). By acting on it with the cyclic generator $\mathbf{g}_c = (P_{8123}8123)$ and the reversing generator $\mathbf{g}_r = (P_{8123})(83)(12)$, we can reproduce all the ten permutations in the equivalent class,²

$$\begin{aligned} \text{V-type : } & (P)(8)(12)(3) , \\ \text{P-type : } & (P8)(132) , (P3)(812) , \\ \text{Bad : } & (P)(38)(1)(2) , (P231)(8) , (P182)(3) , \\ & (P823)(1) , (P318)(2) , (P1)(832) , (P2)(813) . \end{aligned} \quad (3.8)$$

From the V-type cycle representation $(P_{8123})(8)(12)(3)$, we see immediately the quartic vertex structure

$$(P_{8123})(8)(12)(3) \implies P_{8123} \begin{array}{c} 8 \\ \diagdown \\ \diagup \\ 3 \end{array} P_{12} , \quad (3.9)$$

²We omit the subscript in the propagator P when there is no possible confusion.

where the $\{P_{12}, 1, 2\}$ part is another cubic vertex, following the analysis of (3.7). Thus we get the contribution $\left(\frac{1}{s_{812}} + \frac{1}{s_{123}}\right)$. When combining with (3.6), we do get the complete result (3.3). The above calculation shows that by recursively looking into the V-type cycle representations of each substructure, we can reproduce the full Feynman diagram result.

Now we move to the P-type cycle representation, for example, the planar separation (132)|(4875)(6). We need to analyze the two substructures given by cycle representations $(P_{123})(132)$ and $(P_{123})(4875)(6)$. Using the algorithm given in (2.6), the substructure $(P_{123})(132)$ gives the following eight equivalent cycle representations

$$\begin{aligned} \text{V-type : } & (1)(2)(3P) \quad , \quad (12)(3)(P) \quad , \\ \text{Bad : } & (132)(P) \quad , \quad (1P23) \quad , \quad (124)(3) \quad , \quad (1P3)(2) \quad , \quad (132P) \quad , \quad (1)(23P) \quad , \end{aligned}$$

in which either $(1)(2)(3P_{123})$ or $(12)(3)(P_{123})$ manifests the pole structure $\frac{1}{s_{12}s_{123}}$. Similarly, the substructure $(P_{123})(4875)(6)$ gives the following 12 equivalent cycle representations

$$\begin{aligned} \text{V-type : } & (8P)(4)(56)(7) \quad , \quad (8)(P)(47)(5)(6) \quad , \\ \text{P-type : } & (78P)(456) \quad , \quad (4P8)(765) \quad , \\ \text{Bad : } & (P)(6)(4875) \quad , \quad (P764)(58) \quad , \quad (P5)(47)(68) \quad , \quad (P6)(4578) \quad , \quad (P467)(5)(8) \quad , \\ & (P48675) \quad , \quad (P6)(4)(58)(7) \quad , \quad (P54687) \quad . \end{aligned}$$

From both the V-type cycle representation, we can read out the contribution $\frac{1}{s_{56}s_{1238}} \left(\frac{1}{s_{456}} + \frac{1}{s_{567}}\right)$. Putting two substructures together, we get only two terms

$$\frac{1}{s_{12}s_{56}s_{1238}} \frac{1}{s_{123}} \left(\frac{1}{s_{456}} + \frac{1}{s_{567}} \right) \quad ,$$

compared to the full result (3.3). One can check that only by combining with another P-type cycle representation (128)(3476)(5) can we obtain the full result.

With the above example in mind, let us move on to the systematic investigation of four, five and six point PT-factors. For presentation purpose, we shall organize the independent PT-factors into categories according to the topology of corresponding Feynman diagrams. In the same category, different PT-factors are related by group actions, and can be analyzed in the same manner. Concretely, we can define the group action as follows. In the space of $\frac{n!}{2^n}$ equivalent classes $\mathfrak{b}[\beta]$, we define the permutation action

$$\mathcal{C}(\mathfrak{b}[\beta]) = \mathfrak{b}[\beta|_{i \rightarrow i+1}] \quad , \quad \mathcal{R}(\mathfrak{b}[\beta]) = \mathfrak{b}[\beta|_{i \rightarrow n+1-i}] \quad , \quad (3.10)$$

where \mathcal{C} and \mathcal{R} also generate a dihedral group \mathcal{D}_n .³ The action of \mathcal{D}_n further separates the space of $\mathfrak{b}[\beta]$ into different orbits. The number of elements inside each orbit depends on the symmetric property of such orbit.

³We note that this \mathcal{D}_n is different from the D_n defined in §2 that generates the equivalent class $\mathfrak{b}[\beta]$, since their actions on the permutations are different.

For example, the identity permutation $\text{PT}(\boldsymbol{\beta}) = \langle 12 \cdots n \rangle$ is invariant under \mathcal{D}_n action such that it forms a one dimensional orbit by itself. A nontrivial example is that by acting \mathcal{D}_n onto $\text{PT}(\boldsymbol{\beta}) = \langle 12846573 \rangle$, we get an orbit with four elements:

$$\langle 12846573 \rangle \quad , \quad \langle 13248675 \rangle \quad , \quad \langle 15342687 \rangle \quad , \quad \langle 17354628 \rangle . \quad (3.11)$$

The above discussion is useful because, all PT-factors in the same orbit of \mathcal{D}_n share the same structure of the cycle representations. Most importantly, starting from the V-type and P-type cycle representations of one PT-factor in the orbit, we can get the V-type and P-type cycle representations of all the other PT-factors in this orbit simply by the mapping $i \mapsto i + 1$ or $i \mapsto n + 1 - i$. Later on we will only study one PT-factor for each orbit.

After above general discussion, we present more example to further elaborate our algorithm. In appendix A, we will give some further discussions on the cycle structure of PT-factors and Feynman diagrams.

3.1 The three and four point cases

At three point, there is only one independent PT-factor $\text{PT}(\boldsymbol{\beta}) = \langle 123 \rangle$. Among the six cycle representations of the equivalent class, only $(1)(2)(3)$ is a good one. The planar separation $(1)|(2)|(3)$ indicates pictorially that the three external legs are attached to a single cubic vertex. This Feynman diagram evaluates to 1, which agrees with the CHY integration result.

At four point, there are three independent PT-factors $\text{PT}(\boldsymbol{\beta})$. Each of them corresponds to an equivalent class with 8 permutations. Their good cycle representations are summarized in the following table as

$\text{PT}(\boldsymbol{\beta})$	V-type	P-type
$\langle 1234 \rangle$	$(1)(2)(3)(4)$	$(41)(23)$, $(12)(34)$
$\langle 1243 \rangle$	$(1)(2)(34)$, $(12)(3)(4)$	
$\langle 1324 \rangle$	$(4)(1)(23)$, $(41)(2)(3)$	

For the PT-factor $\langle 1234 \rangle$, we can read out the complete vertex information from the sole V-type cycle representation $(1)(2)(3)(4)$. This PT-factor gives all trivalent four point Feynman diagrams whose four external legs are connected at cubic vertices respecting the color ordering, and the result is simply $\frac{1}{s_{12}} + \frac{1}{s_{23}}$. In the language of planar separation, the V-type cycle representation can be separated into four parts $(1)|(2)|(3)|(4)$, which can be explained as defining an effective quartic vertex with exactly the same meaning as mentioned above. This structure will be one of the building blocks for the analysis of higher point Feynman diagrams.

However, the two P-type cycle representations alone only provide partial result. For example, the planar separation of cycle representation $(41)|(23)$ indicates that, legs 2 and 3 are connected to the same cubic vertex while legs 4 and 1 are connected to another, resulting in a contribution of $\frac{1}{s_{23}}$. This is half of the complete answer, and the remaining part is given by the other P-type cycle representation $(12)|(34)$, leading to $\frac{1}{s_{12}}$.

The other two PT-factors $\langle 1243 \rangle$ and $\langle 1324 \rangle$ are related through $i \mapsto i + 1$, i.e., $\langle 1243 \rangle \mapsto \langle 2314 \rangle = \langle 1324 \rangle$. In other words, they belong to the same orbit under \mathcal{D}_4 action. Thus by knowing one, we can obtain the other just by relabeling. For $\langle 1243 \rangle$, the V-type cycle representation with planar separation $(1)|(2)|(34)$ indicates a cubic vertex with three legs $\{1, 2, P_{34}\}$, while $(12)|(3)|(4)$ indicates the other cubic vertex with legs $\{P_{12}, 3, 4\}$. Putting them together, we get the s -channel Feynman diagram evaluated to $\frac{1}{s_{12}}$. Alternatively, we can use just one V-type cycle representation to reproduce the complete result. For example, $(1)(2)(34)$ indicates a cubic vertex represented by $(1)(2)(P_{34})$, and a three point substructure $(P_{34})(3)(4)$. Then by using the three point result, this substructure is nothing but another cubic vertex $(P_{34})(3)(4)$. Thus $(1)(2)(34)$ indeed gives the s -channel diagram. For the V-type cycle representation $(12)(3)(4)$, the analysis is exactly the same, and we can show that both V-type cycle representations give the same answer.

3.2 The five point case

For five point case, there are $\frac{5!}{10} = 12$ independent PT-factors $\text{PT}(\beta)$. They can be divided into following four categories,

- (1) The PT-factor $\langle 12345 \rangle$ has only one V-type cycle representation $(1)(2)(3)(4)(5)$ and five P-type cycle representations $(15)(24)(3)$, $(1)(25)(34)$, $(12)(35)(4)$, $(13)(2)(45)$ and $(14)(5)(23)$. The V-type one corresponds to the Feynman diagrams where the legs $\{1, 2, 3, 4, 5\}$ form all possible Feynman diagrams connected by cubic vertices, while respecting the color ordering. The result is simply

$$\begin{array}{c} 2 \\ | \\ 1 \text{---} \text{---} \text{---} 3 \\ / \quad \backslash \\ 5 \quad 4 \end{array} \implies \frac{1}{s_{12}s_{34}} + \frac{1}{s_{23}s_{45}} + \frac{1}{s_{34}s_{51}} + \frac{1}{s_{45}s_{12}} + \frac{1}{s_{51}s_{23}} . \quad (3.12)$$

In the language of planar separations, $(1)|(2)|(3)|(4)|(5)$ indicates an effective five point vertex with the same meaning. As a comparison, each P-type cycle representation corresponds to only two trivalent Feynman diagrams. For example, the planar separation $(15)|(24)(3)$ fixes the pole s_{15} . The substructure $(P_{15})(24)(3)$ has a V-type cycle representation $(P)(2)(3)(4)$ in its equivalent class, indicating an effective quartic vertex, which gives two trivalent Feynman diagrams. Only after combining all the five P-type cycle representations do we get the complete answer, where each Feynman diagram appears twice.

- (2) The following five PT-factors $\langle 12354 \rangle$, $\langle 12435 \rangle$, $\langle 12543 \rangle$, $\langle 13245 \rangle$ and $\langle 14325 \rangle$ form an orbit under \mathcal{D}_5 action, and are related by the cyclic permutation $i \mapsto i + 1$, for example, $\langle 12354 \rangle \mapsto \langle 23415 \rangle = -\langle 14325 \rangle$.⁴ Thus we only need to analyze one of them, say, $\langle 12354 \rangle$. In its equivalent class, There are two V-type cycle representations $(1)(2)(3)(45)$ and $(13)(2)(4)(5)$, together with two P-type cycle representations $(12)(345)$ and $(154)(23)$. For the first V-type cycle representation, the planar separation

⁴One can easily check that the result of $i \mapsto n + 1 - i$ is also in this orbit.

(1)|(2)|(3)|(45) indicates an effective quartic vertex, labeled as V_1 in Eq. (3.13), while for the second V-type cycle representation, the planar separation (13)(2)|(4)|(5) indicates a cubic vertex labeled as V_2 in Eq. (3.13). Putting them together, we do reproduce the unique effective Feynman diagram with five external legs,

$$\begin{array}{c} 3 \\ | \\ \bullet \\ \text{V}_1 \\ | \\ 1 \\ \text{---} \bullet \text{---} \text{---} \bullet \text{---} \\ \text{V}_2 \\ \diagup \quad \diagdown \\ 4 \quad 5 \end{array} \implies \frac{1}{s_{45}} \left(\frac{1}{s_{12}} + \frac{1}{s_{23}} \right) . \quad (3.13)$$

Alternatively, we can obtain the same answer by using only one V-type cycle representation, for instance the planar separation (1)|(2)|(3)|(45). We first replace the cycle (45) by the propagator (P_{45}). This gives the effective quartic vertex V_1 marked in Eq. (3.13) and a three point substructure (P_{45})(45). Then following the three point analysis presented at the beginning of §3.1, we reproduce the vertex V_2 in Eq. (3.13). The complete result can be arrived by combining the two vertices along the propagator P_{45} , which is just Eq. (3.13).

- (3) The following five PT-factors $\langle 12453 \rangle$, $\langle 12534 \rangle$, $\langle 13254 \rangle$, $\langle 13425 \rangle$ and $\langle 14235 \rangle$ form another orbit under \mathcal{D}_5 action, and are related by the cyclic permutation $i \mapsto i + 1$. As before, we only consider the PT-factor $\langle 12453 \rangle$ as example. It contains three V-type cycle representations, and the planar separations (1)|(2)|(345), (12)|(3)|(45) and (321)|(4)|(5) manifest three cubic vertices. After combining them together, we get the effective Feynman diagram

$$\begin{array}{c} 3 \\ | \\ \bullet \\ \text{V}_2 \\ \diagup \quad \diagdown \\ 2 \quad 4 \\ \text{---} \bullet \text{---} \text{---} \bullet \text{---} \text{---} \bullet \text{---} \\ \text{V}_1 \quad \text{V}_3 \\ \diagdown \quad \diagup \\ 1 \quad 5 \end{array} \implies \frac{1}{s_{12}s_{45}} . \quad (3.14)$$

Next, we show how to reproduce above result by using only one V-type cycle representation, for example, (12)(3)(45). The planar separation (12)|(3)|(45) indicates a cubic vertex (P_{12})(3)(P_{45}), which is the vertex V_2 in (3.14). We also get two three point substructures (P_{12})(12) and (P_{45})(45), leading to the vertex V_1 and V_3 respectively in (3.14). The Feynman diagram thus contains only cubic vertices, and there are exactly two internal propagators P_{12} and P_{45} , evaluating to $\frac{1}{s_{12}s_{45}}$. Also, the same result can be obtained by using the planar separation (1)|(2)|(345), where the vertex V_1 in (3.14) is manifest. For the substructure (P_{345})(345), we need to look into its equivalent class. Now using (2.6), we find two V-type cycle representations (P)(3)(45) and ($P3$)(4)(5). According to the four point analysis in §3.1, they both lead to a pole $\frac{1}{s_{45}}$. Thus we get again the result $\frac{1}{s_{12}s_{45}}$.

- (4) The cycle representations for the last PT-factor $\langle 13524 \rangle$ are

$$\begin{aligned} & (1)(2354) \quad , \quad (2)(3415) \quad , \quad (3)(4521) \quad , \quad (4)(5132) \quad , \quad (5)(1243) \quad , \\ & (1)(2453) \quad , \quad (2)(3514) \quad , \quad (3)(4125) \quad , \quad (4)(5231) \quad , \quad (5)(1342) \quad . \end{aligned} \quad (3.15)$$

There is no good cycle representation at all, so the contribution is zero, which is indeed the case.

3.3 The six point case

There are in total $\frac{6!}{12} = 60$ independent PT-factors for the six point case. According to the number of trivalent Feynman diagrams they evaluate to, we can distribute them into different groups, with the number of PT-factors in each group as

# of trivalent Feyn. diagrams	14	5	4	2	1	0
# of PT-factors	1	6	3	21	14	15

(3.16)

We will study them group by group in the following paragraphs.

With 14 Feynman diagrams: There is only one PT-factor $\text{PT}(\beta) = \langle 123456 \rangle$ that evaluates to 14 Feynman diagrams. In the equivalent class, the good cycle representations are

$$\text{V-type : } (1)(2)(3)(4)(5)(6) , \quad (3.17a)$$

$$\begin{aligned} \text{P-type : } (61)(25)(34) , (12)(36)(45) , (23)(41)(56) , \\ (1)(26)(35)(4) , (2)(31)(46)(5) , (3)(42)(15)(6) . \end{aligned} \quad (3.17b)$$

The sole V-type one indicates that the six external legs form all possible cubic diagrams respecting the color ordering, contributing to 14 terms,

$$\begin{aligned} \begin{array}{c} 2 \quad 3 \\ \diagdown \quad \diagup \\ 1 \text{---} \text{---} 4 \\ \diagup \quad \diagdown \\ 6 \quad 5 \end{array} \implies \frac{1}{s_{16}s_{23}s_{45}} + \frac{1}{s_{12}s_{34}s_{56}} + \frac{1}{s_{12}s_{45}s_{123}} + \frac{1}{s_{23}s_{45}s_{123}} + \frac{1}{s_{12}s_{56}s_{123}} \\ + \frac{1}{s_{23}s_{56}s_{123}} + \frac{1}{s_{12}s_{34}s_{126}} + \frac{1}{s_{16}s_{34}s_{126}} + \frac{1}{s_{12}s_{45}s_{126}} + \frac{1}{s_{16}s_{45}s_{126}} \\ + \frac{1}{s_{16}s_{23}s_{156}} + \frac{1}{s_{16}s_{34}s_{156}} + \frac{1}{s_{23}s_{56}s_{156}} + \frac{1}{s_{34}s_{56}s_{156}} . \end{aligned} \quad (3.18)$$

Again, the planar separation $(1)|(2)|(3)|(4)|(5)|(6)$ tells us that the above 14 terms in (3.18) can be effectively represented by a six point vertex, which becomes a building block for higher point analysis.

The P-type cycle representations have two different structures, collected respectively in the first and second row of (3.17b). Among the three cycle representations in the first row, we study $(61)(25)(34)$ as an example. First, the planar separation $(61)|(25)(34)$ gives a cubic vertex with legs $\{6, 1, P_{61}\}$, and a five point substructure $(P_{61})(25)(34)$. In its equivalent class, we have a V-type cycle representation $(P_{61})(2)(3)(4)(5)$, indicating that the substructure is just an effective five point vertex. Thus from the planar separation $(61)|(25)(34)$, we reproduce five terms in Eq. (3.18) that contain the pole s_{61} . Similarly, the planar separation $(61)(25)|(34)$ gives a propagator s_{34} and a substructure $(P_{34})(61)(25)$, which has a V-type cycle representation $(P_{34})(5)(6)(1)(2)$. Thus this substructure is another effective five point vertex,

which means that the planar separation (61)(25)|(34) gives another five terms in Eq. (3.18) that contain the pole s_{34} . They have two common terms to the result of the first planar separation, so the P-type cycle representation (61)(25)|(34) gives eight terms in Eq. (3.18). If we combine the contributions from all the three P-type ones in the first row of (3.17b) and remove the overlaps, we get the complete answer (3.18).

Finally, each of the three cycle representations in the second row of (3.17b) gives four terms in Eq. (3.18). For example, the planar separation (1)(26)|(35)(4) gives a propagator s_{612} , together with two four point substructures (P)(1)(26) and (P)(35)(4). In their equivalent classes, the former has a V-type cycle representation (P)(6)(1)(2) while the latter has (P)(3)(4)(5), both of which are effective quartic vertices, so that their contribution is

$$(1)(26)|(35)(4) \implies \frac{1}{s_{612}} \left(\frac{1}{s_{12}} + \frac{1}{s_{61}} \right) \left(\frac{1}{s_{34}} + \frac{1}{s_{45}} \right). \quad (3.19)$$

Summing over the contributions of these three P-type cycle representations, we reproduce the twelve terms in Eq. (3.18) that contain a three-particle pole s_{ijk} .

With 5 Feynman diagrams: There are six PT-factors in this category,

$$\langle 123465 \rangle, \quad \langle 123546 \rangle, \quad \langle 124356 \rangle, \quad \langle 126543 \rangle, \quad \langle 132456 \rangle, \quad \langle 154326 \rangle. \quad (3.20)$$

The last five PT-factors can be generated from the first one by cyclic permutation $i \mapsto i+1$. They actually form an orbit under \mathcal{D}_6 action. In the equivalent class of $\langle 123465 \rangle$, the good cycle representations are

$$\begin{aligned} \text{V-type:} & \quad (1)(2)(3)(4)(56), \quad (14)(23)(5)(6), \\ \text{P-type:} & \quad (1526)(34), \quad (3546)(12), \quad (13)(2)(456), \quad (24)(3)(165). \end{aligned} \quad (3.21)$$

We first derive the result by combining the information from all the V-type cycle representations. From previous examples, we can easily tell that the planar separation (1)|(2)|(3)|(4)|(56) indicates an effective five point vertex while (14)(23)|(5)|(6) indicates a cubic vertex. Thus we have fixed the effective Feynman diagram and obtain following result,

$$\begin{array}{c} 4 \\ | \\ 3 \text{ --- } \text{---} \\ | \\ 2 \text{ --- } \text{---} \\ | \\ 1 \end{array} \begin{array}{c} \diagup 5 \\ \text{---} \\ \diagdown 6 \end{array} \implies \frac{1}{s_{56}} \left(\frac{1}{s_{12}s_{34}} + \frac{1}{s_{12}s_{123}} + \frac{1}{s_{23}s_{123}} + \frac{1}{s_{23}s_{156}} + \frac{1}{s_{34}s_{156}} \right). \quad (3.22)$$

As an alternative approach, we repeat the result by using only one V-type cycle representation and recursively those of substructures. For example, besides the cubic vertex, the separation (14)(23)|(5)|(6) also indicates a substructure (P)(14)(23), which has the V-type cycle representation (P)(1)(2)(3)(4) in its equivalent class generated by (2.6). Thus we again recover the effective five point vertex.

Alternatively, let us use the P-type cycle representations to find the result. There are two different structures (1526)|(34) and (3546)|(12) manifest a two-particle pole, while (13)(2)|(456) and (24)(3)|(165)

manifest a three-particle pole. In the first class, the substructure $(P)(1526)$ gives the V-type cycle representation $(P)(56)(1)(2)$ after using (2.6), so we have

$$(1526)|(34) \implies \frac{1}{s_{34}s_{56}} \left(\frac{1}{s_{12}} + \frac{1}{s_{561}} \right). \quad (3.23)$$

Similarly, we can derive that

$$(3546)|(12) \implies \frac{1}{s_{12}s_{56}} \left(\frac{1}{s_{34}} + \frac{1}{s_{123}} \right). \quad (3.24)$$

For $(13)(2)|(456)$ and $(24)(3)|(165)$, similar analysis applies for each substructure, we find that

$$(13)(2)|(456) \implies \frac{1}{s_{456}s_{56}} \left(\frac{1}{s_{12}} + \frac{1}{s_{23}} \right), \quad (24)(3)|(165) \implies \frac{1}{s_{561}s_{56}} \left(\frac{1}{s_{23}} + \frac{1}{s_{34}} \right). \quad (3.25)$$

The complete result can only be recovered by combining all four P-type contributions.

With 4 Feynman diagrams: There are three PT-factors $\langle 123654 \rangle$, $\langle 125436 \rangle$ and $\langle 143256 \rangle$ that evaluate to four Feynman diagrams. They are related by the cyclic permutation $i \mapsto i + 1$, and form an orbit under \mathcal{D}_6 action. Let us take $\langle 123654 \rangle$ as an example. The good cycle representations are

$$\begin{aligned} \text{V-type:} & \quad (1)(2)(3)(46)(5) \quad , \quad (13)(2)(4)(5)(6) \quad , \\ \text{P-type:} & \quad (1432)(56) \quad , \quad (1236)(45) \quad , \quad (12)(3456) \quad , \quad (23)(1654) \quad . \end{aligned}$$

In the V-type cycle representations, the planar separation $(1)|(2)|(3)|(46)(5)$ indicates an effective quartic vertex with legs $\{1, 2, 3, P_{456}\}$, while the planar separation $(13)(2)|(4)|(5)|(6)$ indicates another effective quartic vertex with legs $\{4, 5, 6, P_{123}\}$. By combining them, we get an effective Feynman diagram with two quartic vertices, evaluated to

$$\begin{array}{c}
 \begin{array}{ccc}
 & 3 & 4 \\
 & | & | \\
 2 & - & | & - & 5 \\
 & | & | \\
 & 1 & 6
 \end{array}
 & \implies &
 \frac{1}{s_{12}s_{123}s_{45}} + \frac{1}{s_{12}s_{123}s_{56}} + \frac{1}{s_{23}s_{123}s_{45}} + \frac{1}{s_{23}s_{123}s_{56}} .
 \end{array} \quad (3.26)$$

We can also arrive at above result by analyzing just one V-type cycle representation with its substructures. For $(1)|(2)|(3)|(46)(5)$, the substructure $(P)(46)(5)$ has an equivalent V-type cycle representation $(P)(4)(5)(6)$ in the equivalent class generated by (2.6), so we recover the result (3.26). If we start from $(13)(2)|(4)|(5)|(6)$, the analysis is similar.

For the P-type cycle representations, each one contributes two terms in (3.26). For example, the planar separation $(12)|(3456)$ gives a pole s_{12} and a substructure $(P_{12})(3456)$, and the substructure has an equivalent V-type cycle representation $(P_{12})(3)|(5)(46)$ in the equivalent class. We can then read

out the pole s_{456} and another substructure $(P_{456})(5)(46)$. This substructure further gives a V-type cycle representation $(P_{456})(4)(5)(6)$, indicating a quartic effective vertex. Putting them together, we get

$$(12)|(3456) \implies \frac{1}{s_{12}s_{456}} \left(\frac{1}{s_{45}} + \frac{1}{s_{56}} \right). \quad (3.27)$$

Similar analysis can be done for other three P-type cycle representations, and the results are

$$\begin{aligned} (1432)|(56) &\implies \frac{1}{s_{56}s_{123}} \left(\frac{1}{s_{12}} + \frac{1}{s_{23}} \right), \\ (1236)|(45) &\implies \frac{1}{s_{45}s_{123}} \left(\frac{1}{s_{12}} + \frac{1}{s_{23}} \right), \\ (1654)|(23) &\implies \frac{1}{s_{23}s_{456}} \left(\frac{1}{s_{45}} + \frac{1}{s_{56}} \right). \end{aligned} \quad (3.28)$$

Again, we see that a single P-type cycle representation is not sufficient to provide the complete information, and we need to combine all of them.

With 2 Feynman diagrams: There are 21 PT-factors that evaluate to two Feynman diagrams. According to the action of \mathcal{D}_6 , we can divide them into three orbits as

$$\mathcal{S}_1 : \quad \langle 125643 \rangle, \quad \langle 126534 \rangle, \quad \langle 132546 \rangle, \quad \langle 145326 \rangle, \quad \langle 124365 \rangle, \quad \langle 154236 \rangle, \quad (3.29a)$$

$$\mathcal{S}_2 : \quad \langle 126453 \rangle, \quad \langle 132465 \rangle, \quad \langle 153426 \rangle, \quad (3.29b)$$

$$\begin{aligned} \mathcal{S}_3 : \quad &\langle 123645 \rangle, \quad \langle 143265 \rangle, \quad \langle 134526 \rangle, \quad \langle 124563 \rangle, \quad \langle 142356 \rangle, \quad \langle 125346 \rangle, \\ &\langle 123564 \rangle, \quad \langle 152346 \rangle, \quad \langle 126345 \rangle, \quad \langle 132654 \rangle, \quad \langle 134256 \rangle, \quad \langle 124536 \rangle. \end{aligned} \quad (3.29c)$$

For the category \mathcal{S}_1 of (3.29), we take $\langle 125643 \rangle$ as an example. The good cycle representations are

$$\text{V-type:} \quad (12)(3)(4)(56), \quad (1)(2)(3546), \quad (1423)(5)(6),$$

$$\text{P-type:} \quad (132)(456), \quad (15)(26)(34).$$

The planar separations in the V-type cycle representations indicate the following vertex structures,

$$(12)|(3)|(4)|(56) \implies \text{quartic vertex with legs } P_{12}, 3, 4, \text{ and } P_{56}, \quad (3.30a)$$

$$(1)|(2)|(3546) \implies \text{cubic vertex with legs } 1, 2, \text{ and } P_{12}, \quad (3.30b)$$

$$(1423)|(5)|(6) \implies \text{cubic vertex with legs } 5, 6, \text{ and } P_{56}. \quad (3.30c)$$

Combining them together, we get an effective Feynman diagram with two cubic vertices and one quartic vertex, and the result is

$$\begin{array}{c} \begin{array}{c} 3 \quad 4 \\ \diagdown \quad / \\ \text{---} \\ / \quad \diagdown \\ 2 \quad 5 \\ | \quad | \\ 1 \quad 6 \end{array} \implies \frac{1}{s_{12}s_{56}} \left(\frac{1}{s_{123}} + \frac{1}{s_{34}} \right). \end{array} \quad (3.31)$$

We can also reproduce above result by considering only one V-type cycle representation and its substructures. For example, the planar separation $(1)|(2)|(3546)$ gives the substructure $(P)(3546)$, which has a V-type cycle representation $(P)(3)(4)(56)$ generated by (2.6). Thus the substructure contains a quartic vertex with legs P_{12} , 3, 4, P_{56} , and a cubic vertex with legs 5, 6, P_{56} .

Alternatively, let us discuss the contribution from P-type cycle representation. For the one $(132)|(456)$, we can derive two substructure of V-type cycle representations $(P)(12)(3)$ and $(P)(4)(56)$. Thus we get the contribution $\frac{1}{s_{12}s_{56}s_{123}}$. Similarly, the P-type cycle representation $(15)(26)|(34)$ has a substructure $(P)(15)(26)$ that has a V-type cycle representation $(P)(12)(56)$. Thus we get the contribution $\frac{1}{s_{12}s_{34}s_{56}}$. Again, we need to combine the information of all the P-type cycle representations to get the full result.

Next, we move to the category \mathcal{S}_2 of (3.29), and take $\langle 126453 \rangle$ as an example. The good cycle representations are

$$\begin{aligned} \text{V-type :} & \quad (1)(2)(36)(4)(5) \quad , \quad (12)(3)(45)(6) \quad , \\ \text{P-type :} & \quad (132)(465) \quad , \quad (126)(345) \quad . \end{aligned}$$

The V-type cycle representation $(1)(2)(36)(4)(5)$ allows two different planar separations $(1)|(2)|(36)(4)(5)$ and $(1)(2)(36)|(4)|(5)$, so it gives two cubic vertices. Meanwhile, $(12)(3)(45)(6)$ has only one planar separation $(12)|(3)|(45)|(6)$, so it gives an effective quartic vertex. Putting all these vertices together, we get the effective Feynman diagram

$$\begin{array}{c} \begin{array}{c} 3 \\ | \\ 2 \quad \diagdown \quad \diagup \quad 4 \\ | \quad \quad \quad | \\ 1 \quad \diagup \quad \diagdown \quad 5 \\ | \\ 6 \end{array} \implies \frac{1}{s_{12}s_{45}} \left(\frac{1}{s_{123}} + \frac{1}{s_{612}} \right) . \end{array} \quad (3.32)$$

Now we follow another approach by considering only one V-type cycle representation to reproduce the result (3.32). If we focus on the cycle representation $(12)(3)(45)(6)$, the planar separation $(12)|(3)|(45)|(6)$ gives the final result directly. While if we focus on the V-type cycle representation $(1)(2)(36)(4)(5)$, the planar separation $(1)|(2)|(36)(4)(5)$ will manifest the cubic vertex with legs 1, 2, P_{12} , and the substructure $(P)(36)(4)(5)$ then generates a V-type cycle representation $(P)(3)(45)(6)$, which leads to a quartic and a cubic vertex. Hence we do reproduce the result (3.32). Analysis of $(1)(2)(36)(4)(5)$ from the planar separation $(1)(2)(36)|(4)|(5)$ is exactly the same. We note that the P-type cycle representation $(132)|(465)$ gives $\frac{1}{s_{12}s_{45}s_{123}}$ while $(126)|(345)$ gives $\frac{1}{s_{12}s_{45}s_{612}}$. Thus by combining them, we get the complete result.

Finally, we study the category \mathcal{S}_3 of (3.29), and take $\langle 123645 \rangle$ as example. The good cycle representations are

$$\begin{aligned} \text{V-type :} & \quad (1)(2)(3)(465) \quad , \quad (1236)(4)(5) \quad , \quad (13)(2)(45)(6) \quad , \\ \text{P-type :} & \quad (12)(356)(4) \quad , \quad (23)(164)(5) \quad . \end{aligned}$$

Using the V-type cycle representations, we see that $(1)|(2)|(3)|(465)$ gives an effective quartic vertex, while $(1236)|(4)|(5)$ and $(13)(2)|(45)|(6)$ give two cubic vertices. Putting all of them together, we get the effective Feynman diagram

$$\begin{array}{c} \text{3} \\ | \\ \text{---} \\ | \\ \text{1} \end{array}
\begin{array}{c} \\ \text{---} \\ | \\ \text{6} \end{array}
\begin{array}{c} \\ \\ \diagup \\ \diagdown \end{array}
\begin{array}{c} \text{4} \\ \\ \text{5} \end{array}
\Rightarrow \frac{1}{s_{123}s_{45}} \left(\frac{1}{s_{12}} + \frac{1}{s_{23}} \right). \quad (3.33)$$

Alternatively, let us take just one single V-type cycle representation to reproduce above result. From the planar separation $(1)|(2)|(3)|(465)$, the substructure $(P)(465)$ generates a V-type cycle representation $(P)(45)(6)$ according to (2.6). Thus we get the same effective Feynman diagram as in (3.33). From the planar separation $(1236)|(4)|(5)$, the substructure $(P)(1236)$ has a V-type cycle representation $(P6)(1)(2)(3)$, while from $(13)(2)|(45)|(6)$, the substructure $(P)(13)(2)$ gives a V-type cycle representation $(P)(1)(2)(3)$. Both of them recover the result (3.33) respectively.

For the P-type cycle representations, we note that $(12)|(356)(4)$ gives the partial result $\frac{1}{s_{12}s_{123}s_{45}}$ following our algorithm, while $(23)|(164)(5)$ gives another piece $\frac{1}{s_{23}s_{123}s_{45}}$. They combine to give the full result (3.33).

With 1 Feynman diagram: There are 14 PT-factors that evaluate to one Feynman diagram. According to the action of \mathcal{D}_6 , they can be distributed into three orbits,

$$\mathcal{S}_1 : \quad \langle 132645 \rangle, \quad \langle 134265 \rangle, \quad \langle 135426 \rangle, \quad \langle 124653 \rangle, \quad \langle 153246 \rangle, \quad \langle 126435 \rangle, \quad (3.34a)$$

$$\mathcal{S}_2 : \quad \langle 125463 \rangle, \quad \langle 142365 \rangle, \quad \langle 143526 \rangle, \quad \langle 132564 \rangle, \quad \langle 152436 \rangle, \quad \langle 126354 \rangle, \quad (3.34b)$$

$$\mathcal{S}_3 : \quad \langle 125634 \rangle, \quad \langle 145236 \rangle. \quad (3.34c)$$

For the category \mathcal{S}_1 of (3.34), we analyze $\langle 132645 \rangle$ as example. Its good cycle representations are

$$\text{V-type:} \quad (1)(23)(465), \quad (123)(45)(6), \quad (136)(2)(4)(5), \quad (2)(3)(164)(5). \quad (3.35)$$

There is no P-type cycle representation. This can be understood as follows. Since the final result only contains one term, so that we do not have partial result. From the V-type cycle representations, we see that each planar separation of $(1)|(23)|(465)$, $(123)|(45)|(6)$, $(136)(2)|(4)(5)$ and $(2)|(3)|(164)(5)$ indicates a cubic vertex. Thus we get a trivalent Feynman diagram evaluated to

$$\begin{array}{c} \text{2} \quad \text{3} \quad \text{4} \quad \text{5} \\ \diagdown \quad \diagup \quad \diagdown \quad \diagup \\ \text{---} \quad \text{---} \\ | \quad | \\ \text{1} \quad \quad \quad \text{6} \end{array}
\Rightarrow \frac{1}{s_{23}s_{45}s_{123}}. \quad (3.36)$$

Of course, we can get the same result by considering a single V-type cycle representation and its substructures. For example, besides the cubic vertex with legs $\{1, P_{23}, P_{123}\}$, the planar separation $(1)|(23)|(465)$

also indicates a substructure $(P)(465)$, which contains a V-type cycle representation $(P)(45)(6)$, giving exactly the other two cubic vertices in Eq. (3.36). Analysis for the other V-type cycle representations is the same.

For the category \mathcal{S}_2 of (3.34), we analyze $\langle 125463 \rangle$ as example. Its good cycle representations are

$$\text{V-type: } (1)(2)(356)(4) , (132)(45)(6) , (1)(236)(4)(5) , (12)(3)(465) . \quad (3.37)$$

Each planar separation of $(1)|(2)|(356)(4)$, $(132)|(45)|(6)$, $(1)(236)|(4)|(5)$ and $(12)|(3)|(465)$ indicates a cubic vertex. After combining them, we get the trivalent Feynman diagram evaluated to

$$\Rightarrow \frac{1}{s_{12}s_{45}s_{123}} . \quad (3.38)$$

Finally, for the category \mathcal{S}_3 of (3.34), we analyze $\langle 125634 \rangle$ as example. Its good cycle representations are

$$\text{V-type: } (1)(2)(35)(64) , (13)(24)(5)(6) , (15)(26)(3)(4) , (12)(34)(56) . \quad (3.39)$$

Again, all the planar separations $(1)|(2)|(35)(64)$, $(13)(24)|(5)|(6)$, $(15)(26)|(3)|(4)$ and $(12)|(34)|(56)$ indicate cubic vertices, so that the final result is

$$\Rightarrow \frac{1}{s_{12}s_{34}s_{56}} . \quad (3.40)$$

Both Eq. (3.38) and (3.40) can be reproduced by a single V-type cycle representation, and the analysis is almost the same to that of the category \mathcal{S}_1 shown above.

With 0 Feynman diagram: Finally, there are 15 PT-factors that evaluate to zero. According to the action of \mathcal{D}_6 , they can be distributed into three orbits,

$$\mathcal{S}_1 : \quad \langle 124635 \rangle , \langle 146235 \rangle , \langle 134625 \rangle , \langle 136245 \rangle , \langle 135624 \rangle , \langle 135246 \rangle , \quad (3.41a)$$

$$\mathcal{S}_2 : \quad \langle 125364 \rangle , \langle 146325 \rangle , \langle 143625 \rangle , \langle 136254 \rangle , \langle 136524 \rangle , \langle 142536 \rangle , \quad (3.41b)$$

$$\mathcal{S}_3 : \quad \langle 135264 \rangle , \langle 136425 \rangle , \langle 142635 \rangle . \quad (3.41c)$$

The category \mathcal{S}_3 of (3.41) does not have any good cycle representations, and indeed it evaluates to zero.

For the category \mathcal{S}_1 of (3.41), we take $\langle 124635 \rangle$ as example. The good cycle representations are

$$\text{V-type: } (1)(2)(3465) , \quad \text{P-type: } (12)(3564) . \quad (3.42)$$

Both of them manifest a pole P_{12} , together with a substructure $(P)(3465)$ and $(P)(3564)$ respectively. However, both substructures are members of (3.15), which give zero contribution. This can be seen clearly

if we replace P by 2, and then replace $i \rightarrow i - 1$ for the rest. Thus we see that the category \mathcal{S}_1 evaluates to zero because it contains a substructure with zero contribution. Actually, the category \mathcal{S}_2 of (3.41) evaluates to zero for the same reason. For example, $\langle 125364 \rangle$ has good cycle representations

$$\text{V-type : } (1)(2)(3564) \quad , \quad \text{P-type : } (12)(3465) \quad , \quad (3.43)$$

whose substructures are identical to the case of category \mathcal{S}_1 .

This result can also be understood from another point of view. As we have shown with many examples, the V-type cycle representations encode the vertex structure of corresponding effective Feynman diagram. In the current case, there is only one V-type cycle representation and it has only one planar separation of cubic vertex. If we use v_m to denote the number of m -point vertices, we should have the following constraint for all the valid effective Feynman diagrams as

$$\sum_{m=3}^n (m-2)v_m = n - 2 . \quad (3.44)$$

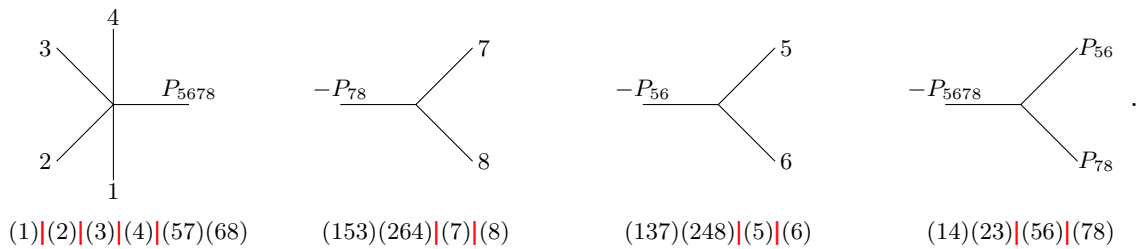
For the cases (3.42) and (3.43), we only have $v_3 = 1$ and all the other $v_i = 0$, while for category \mathcal{S}_3 , all v_i 's are zero. Thus the identity (3.44) is violated, indicating that no such effective Feynman diagram exists. One can check that for all the cases with nonzero results, the identity (3.44) is satisfied.

3.4 Higher point examples

Let us now consider an eight point example with PT-factor $\langle 12347856 \rangle$. It has 16 cycle representations, and we can classify them as

V-type	$(1)(2)(3)(4)(57)(68)$, $(153)(264)(7)(8)$, $(137)(248)(5)(6)$, $(14)(23)(56)(78)$
P-type	$(12)(367458)$, $(13)(2)(468)(5)(7)$, $(175)(24)(3)(6)(8)$, $(34)(185276)$
Bad	(16785432) , $(1874)(25)(36)$, $(1735)(2846)$, $(1456)(27)(38)$ (12347658) , $(1638)(2547)$, $(1)(2648)(357)$, $(1537)(286)(4)$

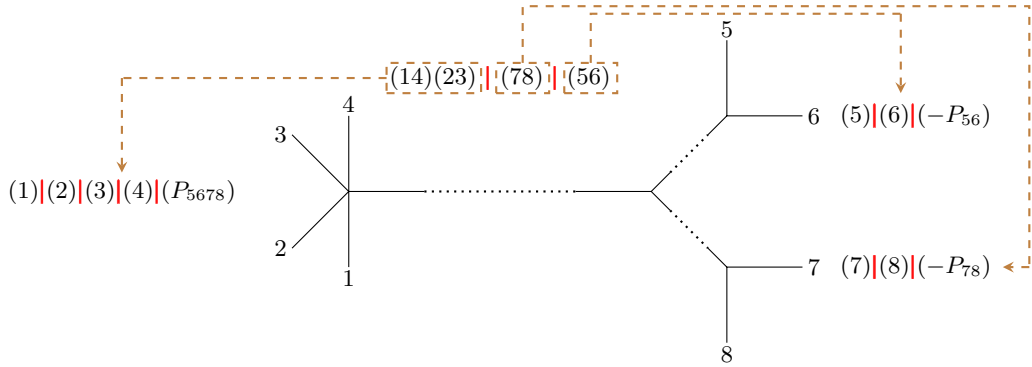
Among them, four are V-type cycle representations, and each one encodes the vertex information. For each cycle representation, there is only one planar separation, and from which we can directly work out



Collectively considering all these four V-type cycle representations, and gluing them via propagators, we get the Feynman diagram as

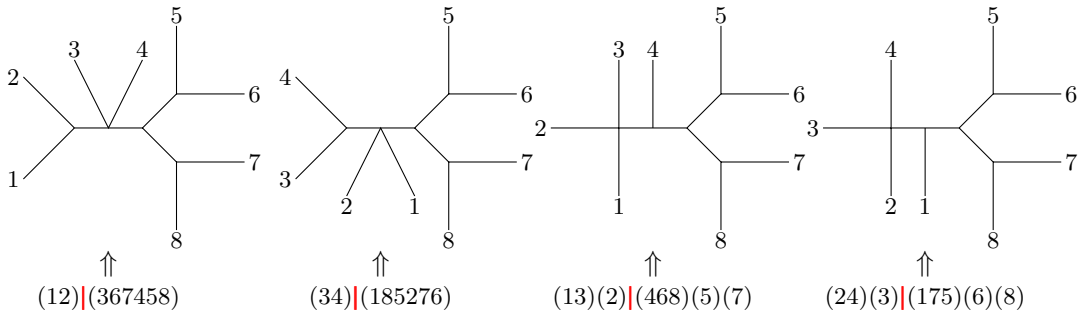
$$\Rightarrow \frac{1}{s_{56}s_{78}s_{1234}} \left(\frac{1}{s_{12}s_{123}} + \frac{1}{s_{23}s_{123}} + \frac{1}{s_{23}s_{234}} + \frac{1}{s_{34}s_{234}} + \frac{1}{s_{12}s_{34}} \right), \quad (3.45)$$

which exactly produces the result of CHY-integrand $\langle 12345678 \rangle \times \langle 12347856 \rangle$. Alternatively, we can reproduce the same result from only one V-type cycle representation by going into its substructures. We use the V-type cycle representation $(14)(23)(56)(78)$ as our example. The planar separation $(14)(23)|(56)|(78)$ gives three substructures, namely $(14)(23)(P_{5678})$, $(56)(P_{56})$ and $(78)(P_{78})$. For each one, we can find a V-type cycle representation that manifests the vertex structure in the equivalent class,



By connecting the substructures together, we obtain the effective Feynman diagram as in (3.45).

There are also four P-type cycle representations. As mentioned previously, they should be considered collectively in order to produce the complete result, while each one only contributes a partial result. From the planar separations of these cycle representations and their substructures, we can work out the contribution of each P-type cycle representation. We will not repeat the detailed analysis here, but only give the result as,

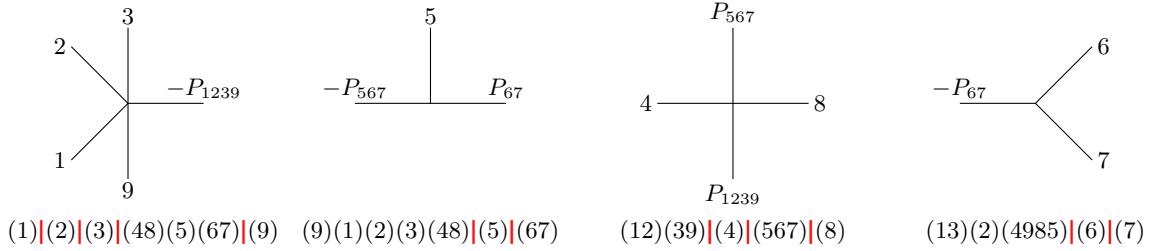


We see that, each P-type cycle representation gives a quartic vertex contained in the original five point vertex. Thus each P-type cycle representation produces two terms. Only after summing up the above four contributions and removing the duplicates can we recover the complete result.

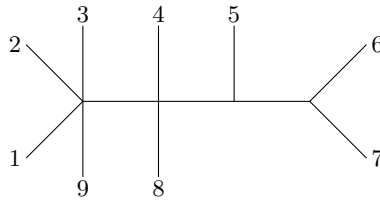
Our last example involves a nine point PT-factor $PT(\beta) = \langle 123857649 \rangle$. There are in all 18 cycle representations and we can classify them as

V-type	$(1)(2)(3)(48)(5)(67)(9)$, $(12)(39)(4)(567)(8)$, $(13)(2)(4985)(6)(7)$
P-type	$(19432)(586)(7)$, $(12389)(457)(6)$, $(19)(247368)(5)$, $(1)(29)(346578)$, $(18764)(23)(59)$
Bad	(142968753) , (163978524) , $(173495)(26)(8)$, $(159836)(27)(4)$, (182546937) (135647928) , $(15)(286974)(3)$, $(1796)(25)(384)$, $(1627)(35)(489)$, $(1458)(2637)(9)$

There are three V-type cycle representations. Each planar separation of V-type cycle representation tells us about the vertex information. The V-type cycle representation $(1)(2)(3)(48)(5)(67)(9)$ allows two different planar separations while each of the other two allow one planar separation. The vertex information of them are presented as follows,



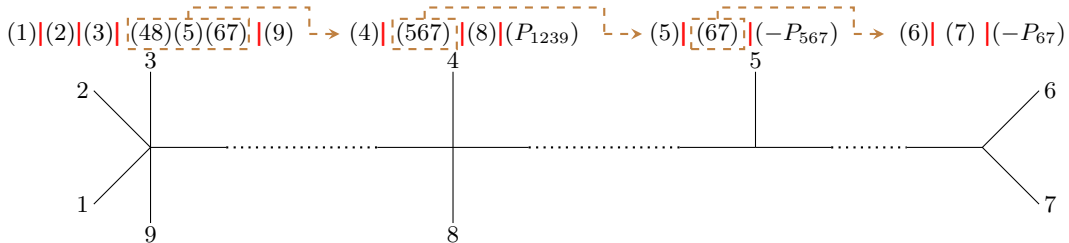
The first planar separation indicates a five point vertex, which corresponds to five possible terms, while the second planar separation indicates a quartic vertex which corresponds to two possible terms. So gluing them together we get the nine point effective Feynman diagram as



which is a collection of 10 trivalent Feynman diagrams, agreeing with the result of the CHY-integrand $\langle 123456789 \rangle \times \langle 123857649 \rangle$.

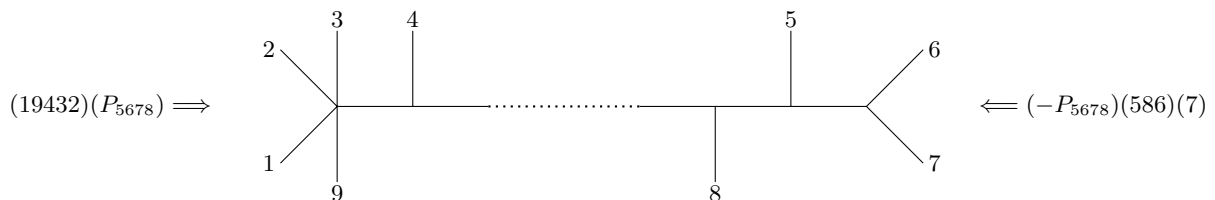
Alternatively, we derive the above result from one V-type cycle representation and its substructures. For instance, the planar separation $(1)|(2)|(3)|(48)(5)(67)|(9)$ indicates a five point vertex, while the substructure $(P_{1239})(48)(5)(67)$ has further structure. By working out the equivalent class of $(P_{1239})(48)(5)(67)$, we find a V-type cycle representation of this substructure that allows the planar separation $(4)|(567)|(8)|(P_{1239})$, indicating a quartic vertex and a four point substructure $(567)(P_{567})$. Then the equivalent V-type cycle representation $(5)|(67)|(P_{567})$ of this four point substructure indicates two cubic vertices with legs 5, P_{67} ,

P_{567} and 6, 7, P_{67} respectively, according to our four point discussion in §3.1. The above recursive process can be graphically represented by



Hence from one V-type cycle representation it is sufficient to obtain the complete result.

On the contrary, if taking only one P-type cycle representation, we will end up with a partial result. For instance, if we take the P-type cycle representation $(19432)(586)(7)$, it has only one planar separation $(19432)|(586)(7)$ that splits the external legs into two parts. For both the substructures $(19432)(P_{5678})$ and $(P_{5678})(586)(7)$, we can work out their contributions by recursively going into their substructures. We will not repeat the details but show the result as follows,



The corresponding effective Feynman diagram obtained by gluing these two subdiagrams contributes only half of the full result, since the leg 4 and 8 is connected in just one way of the two allowed by the quartic vertex $\{P_{9123}, 4, P_{567}, 8\}$ in the original Feynman diagram. We need to include all the P-type cycle representations to reproduce the complete result.

4 From Feynman diagrams to permutations

In §3, we have addressed the problem that given a PT-factor as a permutation acting on the identity element, how we can determine the Feynman diagrams the CHY-integrand evaluated. In this section, we will consider the inverse problem, namely, given an effective Feynman diagram, how to obtain directly the corresponding good cycle representations. We will show that there is a recursive construction to produce the good cycle representations of a given Feynman diagram from the relation between subdiagrams and planar separations. Later, we will use the eight point example given in Fig. 1 to illustrate general discussions. We remind the readers that an m -point vertex in the Feynman diagram stands for the sum of all the m -point trivalent diagrams. For example, a quartic vertex gives the sum of s and t channel trivalent diagrams. The Feynman diagram in Fig. 1a corresponds to the CHY-integrand $\langle 12345678 \rangle \times \langle 12783654 \rangle$, which evaluates

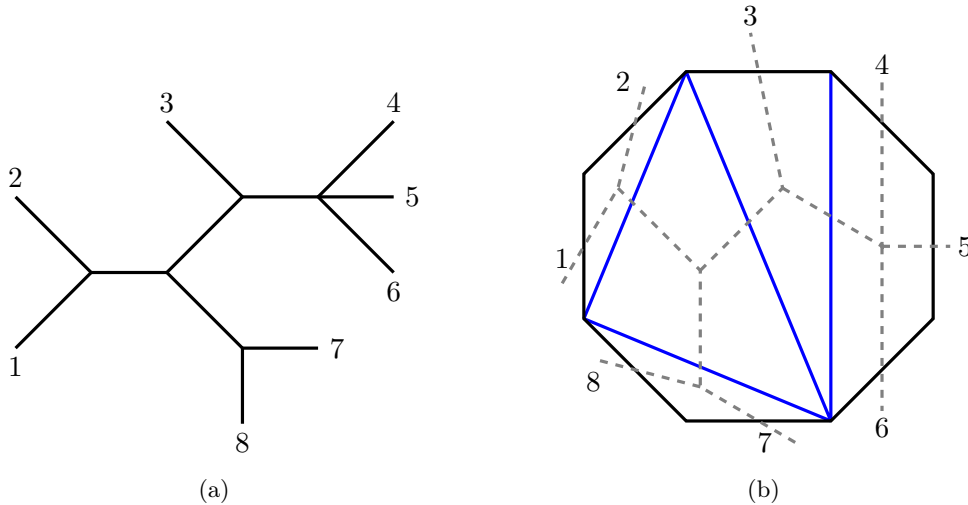


Figure 1: An eight point Feynman diagram and its dual n -gon diagram.

to

$$\frac{1}{s_{12}s_{78}s_{1278}s_{456}} \left(\frac{1}{s_{45}} + \frac{1}{s_{56}} \right). \quad (4.1)$$

As we have mentioned in previous section, the PT-factor $\text{PT}(\beta)$ determines a permutation acting on identity element and it encodes the pole structure of the Feynman diagram. Conversely, the pole structure in the Feynman diagram also encodes the information of permutation. To describe the way of reading out the PT-factor and cycle representations, we find it is more convenient to introduce the polygon with n edges (n -gon) that is dual to the n -point Feynman diagram under inspection.

An n -point effective Feynman diagram can be described as *partial triangulation* of n -gon diagram [31, 33, 34], and an example of our considered eight point Feynman diagram is presented in Fig. 1. Each external leg is dual to an edge of the n -gon, and each vertex is dual to a subpolygon in the interior. A triangulation line inside the n -gon, which cut it into two subpolygons, is dual to a propagator. If the Feynman diagram considered is trivalent diagram with only cubic vertices, the corresponding n -gon is completely triangulated, while if it is an effective Feynman diagram with also higher point vertices, the n -gon diagram is partially triangulated. If we use E_i to denote the number of edges of a subpolygon inside the original n -gon, then the number of terms in the final result is given by

$$\prod_{i \in \text{all polygons}} C(E_i) = \prod_{i \in \text{all polygons}} \frac{2^{E_i-2} (2E_i - 5)!!}{(E_i - 1)!}, \quad (4.2)$$

where $C(n)$ is also the number of all possible n -point color ordered trivalent Feynman diagrams. The blue line in Fig. 1b represents the triangulation of our considered example, and the dashed gray line gives the Feynman diagram dual to the partial triangulation of n -gon. Discussion on the Feynman diagram can as well be applied to the n -gon diagram, and the latter is naturally enrolled in the associahedron [31, 34].

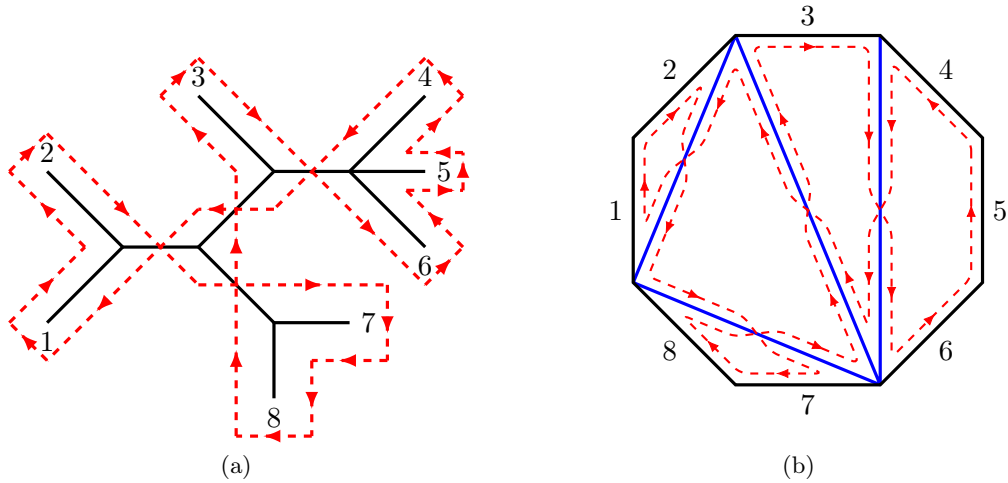


Figure 2: The zig-zag path in an eight point Feynman diagram and n -gon diagram.

4.1 The zig-zag path and cycle-representation of permutation

Now let us return to the problem of reading out the PT-factor from Feynman diagram. A solution for this problem has been provided in paper [15], where a pictorial method has been proposed to write the PT-factor for a given Feynman diagram. Based on their discussion, we will rephrase it by the language of *zig-zag path*.⁵ The basic idea comes as follows,

- Any tree-level Feynman diagram can be placed as a planar diagram, while the external legs lying in the plane apparently define an ordering, identified as PT-factor $\text{PT}(\boldsymbol{\alpha})$.
- Starting from any external leg, we can draw a zig-zag path along the boundary of diagram, which crosses each internal line it meets and closes at the starting point. The ordering of legs along the direction of zig-zag path is identified as PT-factor $\text{PT}(\boldsymbol{\beta})$.

The corresponding CHY-integrand $\text{PT}(\boldsymbol{\alpha}) \times \text{PT}(\boldsymbol{\beta})$ then evaluates to the given Feynman diagram.

The zig-zag path for our considered example is shown in Fig. 2, both in the Feynman diagram and n -gon diagram. In the Feynman diagram, the zig-zag path is along the external legs, while in the n -gon diagram, it is along the interior of edges. In both diagrams, the path crosses the lines whenever they are propagators. It is easy to tell that, for the Feynman diagram shown in Fig. 2, we have $\text{PT}(\boldsymbol{\alpha}) = \langle 12345678 \rangle$, while along the arrows of zig-zag path, we can read out $\text{PT}(\boldsymbol{\beta}) = \langle 12783654 \rangle$, as it should be. However, there are two subtleties we should pay attention to. The PT-factor $\text{PT}(\boldsymbol{\beta}) = \langle 12783654 \rangle$ is obtained under the condition that we read out the zig-zag path from leg 1 towards a specific direction. If starting from the same leg 1 but with opposite direction, we will get $\text{PT}(\boldsymbol{\beta}) = \langle 14563872 \rangle$. If we start from another leg and

⁵More discussions on the zig-zag path can be found in [35–37].

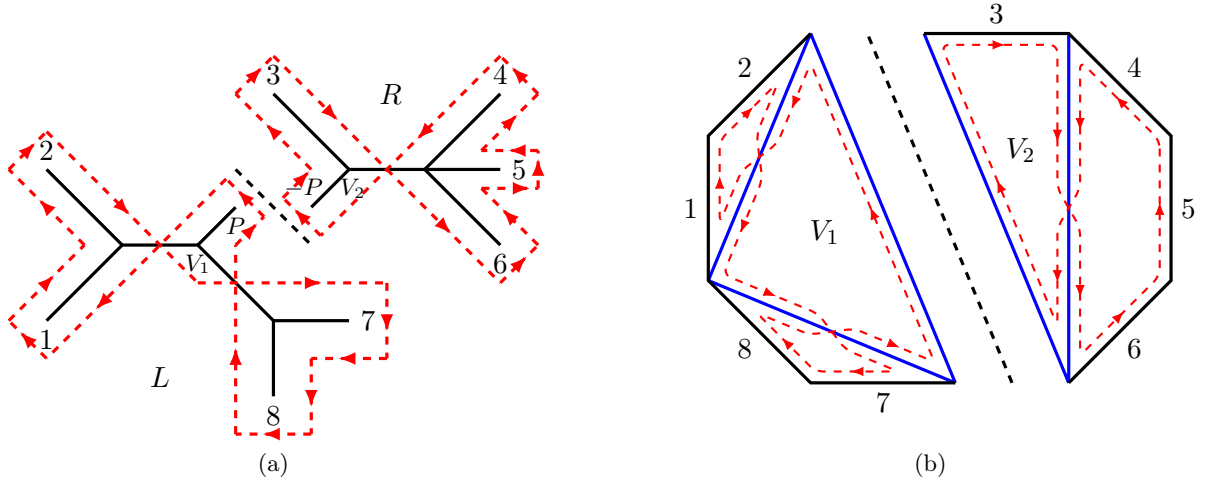


Figure 3: The zig-zag paths of subdiagrams in Feynman diagram and n -gon diagram.

a chosen direction, we will get another PT-factor, though they are in the same equivalent class. Special attention should be paid to the orientation of zig-zag path. It is a local but not global property, and it only make sense with respect to a vertex. For example, for the cubic vertex where legs $\{1, 2\}$ attached to, the zig-zag path around it is clockwise, while for the quartic vertex where legs $\{4, 5, 6\}$ attached to, the zig-zag path around it is anti-clockwise. The orientation of zig-zag path is more obvious in the n -gon diagram, as shown in Fig. 2b. For each polygon inside the n -gon, the zig-zag path can be considered as a closed loop with definite orientation. If the zig-zag path in the triangle with edge 1, 2 is clockwise, then the zig-zag paths in the triangles with legs 7, 8 and with legs 3 are also clockwise, while zig-zag paths in the triangle in middle and the quadrangle are anti-clockwise. To the whole Feynman diagram or n -gon diagram, we do not need to worry about the ambiguity of the zig-zag path orientation, since our canonical definition of PT-factors in §2 fixes which leg to start and which direction it should ahead. However, as we would discuss soon, the orientation of zig-zag path is important in the recursive construction of PT-factors.

Now we consider splitting the Feynman diagram into two subdiagrams (labeled as L and R) at the propagator P_{7812} that connects the vertex V_1 and V_2 , as shown in Fig. 3. In each subdiagram, the zig-zag path form a closed loop, from which we can read out the PT-factors. In order to define the canonical ordering of PT-factors, we read out the α -orderings from both subdiagrams in the clockwise direction as

$$\text{PT}(\alpha_L) = \langle 7812P \rangle \quad , \quad \text{PT}(\alpha_R) = \langle P3456 \rangle \quad . \quad (4.3)$$

Next, we read out $\text{PT}(\beta_{L,R})$ from the zig-zag paths of both subdiagrams, starting from the leg P . We emphasize that the zig-zag path for subdiagram L is anti-clockwise with respect to the vertex V_1 , while the zig-zag path for subdiagram R is clockwise with respect to V_2 . The orientations of two zig-zag paths are always opposite with respect to the two vertices connect by the split propagator. This is a generic and

important feature since, as we mentioned before, the orientations of zig-zag paths of two adjacent polygons in the n -gon diagram are always opposite. This feature will play a consequential role in determining the cycle representations for subdiagrams. Now we write down the PT-factors for the subdiagrams according to the arrows in the zig-zag paths of Fig. 3a as

$$\text{PT}(\beta_L) = \langle P1278 \rangle \quad , \quad \text{PT}(\beta_R) = \langle P3654 \rangle \quad . \quad (4.4)$$

The complete $\text{PT}(\beta)$ is given by the union of (4.4) in a specific way: $\langle 1278P \rangle \oplus \langle P3654 \rangle \rightarrow \langle 12783654 \rangle$. The pattern will be clear if we use their cycle representation,

$$\text{PT}(\beta_L) = \langle P1278 \rangle \sim (P)(17)(28) \quad , \quad \text{PT}(\beta_R) = \langle P3654 \rangle \sim (P)(3)(46)(5) \quad . \quad (4.5)$$

Namely, we can obtain a V-type cycle representation of the complete Feynman diagram by the union of the above two after eliminating the single cycle (P) : $(17)(28)(P) \oplus (P)(3)(46)(5) = (17)(28)(3)(46)(5)$.⁶

To obtain the above result, we have to select two specific cycle representations for the subdiagrams out of the 10 equivalent ones of $\beta_{L,R}$,

$$\beta_L : \quad \left\{ \begin{array}{ccccc} (P)(17)(28) & (P8127) & (P78)(1)(2) & (P21)(7)(8) & (P1872) \\ (P)(78)(12) & (P17)(8)(2) & (P2718) & (P7281) & (P82)(7)(1) \end{array} \right\} \quad (4.6a)$$

$$\beta_R : \quad \left\{ \begin{array}{ccccc} (P)(3)(46)(5) & (P43)(56) & (P534)(6) & (P635)(4) & (P36)(45) \\ (P)(3456) & (P3)(4)(5)(6) & (P654)(3) & (P5)(364) & (P46)(35) \end{array} \right\} \quad . \quad (4.6b)$$

First of all, we choose those that leave P in a single cycle as (P) in the equivalent class. This is reasonable since when gluing subdiagrams, P should get eliminated without affecting other cycles, which is possible only if P is in a single cycle. This limits us to the two in the first column of (4.6). Next, we need to answer which one to choose among the two. Looking back to (4.5), we find that β_R is a V-type cycle representation that manifests the vertex V_2 , while β_L is not a good cycle representation. If we color the legs according to how they are separated by V_1 and V_2 , then for $\text{PT}(\beta_R)$, we have $(P)(\mathbf{3})(\mathbf{46})(\mathbf{5})$, namely, each cycle contains elements with the same color, i.e., elements from the same part of the V_2 splitting. We say that this cycle representation satisfies *planar splitting* for short. In contrary, for $\text{PT}(\beta_L)$, some cycles contain elements with different colors, i.e., the elements inside one cycle are from different parts of the V_1 splitting. We call it cycle representation *non-planar splitting* for short. One notices that among the two subdiagrams of Fig. 3a, one cycle representation is planar splitting while the other is non-planar splitting. For instance, if the arrows in Fig. 3a is reversed globally, then for $\text{PT}(\beta_L)$ the consequent cycle representation is $(P)(\mathbf{78})(\mathbf{12})$ while for $\text{PT}(\beta_R)$ it is $(P)(\mathbf{3456})$. Again, one cycle representation is planar splitting and the other is non-planar

⁶Now the operation \oplus can be properly defined as follows: if β_1 and β_2 are two permutations that have only one overlap element P , and in both of them P sits in a single cycle, namely, $\beta_{1,2} = (P)\beta'_{1,2}$, we have

$$\beta_1 \oplus \beta_2 = \beta'_1 \beta'_2 \quad .$$

splitting. By gluing them together, we get (78)(12)(3456), which is another V-type cycle representation of the complete Feynman diagram. This feature results from the fact that the orientations of the subdiagram zig-zag paths are opposite with respect to the two vertices connected by the split propagator. It is generally true no matter how we cut the complete Feynman diagram.

The above discussion indicates clearly that the permutation representation of PT-factor can be recursively constructed by breaking a complete Feynman diagram into subdiagrams along internal propagators. We will provide a systematic and abstract construction in next subsection.

4.2 The recursive construction of PT-factor via cycle representation

We already have the experience that, (1) in the gluing of two subdiagrams to one complete diagram, cycle representation of one subdiagram should be planar splitting, and that of the other should be non-planar splitting, (2) the planar splitting cycle representation corresponds to a zig-zag path in clockwise direction, while the non-planar splitting cycle representation corresponds to a zig-zag path in anti-clockwise direction. The orientation of zig-zag path is related to the planar or non-planar splitting of cycle representations because we use the convention that $\text{PT}(\boldsymbol{\alpha})$ is obtained by traversing the external legs in clockwise direction.

Let us head to a more systematic and abstract discussion on the recursive construction of cycle representation for a Feynman diagram. Consider a generic n -point effective Feynman diagram, where besides cubic vertices, the effective ($m > 3$)-point vertices can also appear. An m -point vertex represents a collection of all possible $\frac{(2m-4)!}{(m-1)!(m-2)!}$ such m -point trivalent subdiagrams. If we use v_m to denote the number of m -point vertices appearing in the effective Feynman diagram, then they should satisfy the constraint

$$\sum_{m=3}^n (m-2)v_m = n-2, \quad (4.7)$$

where the total number of vertices $\sum v_m$ falls between 1 and $n-2$. An illustration of the n -point Feynman diagram as well as the dual n -gon diagram with also the zig-zag path is shown in Fig. 4.

Let us focus on a m -point vertex, marked as a black dot in the middle of the blue octagon⁷ in Fig. 4. This vertex connects m subdiagrams via m propagators P_k with $k = 1, 2, \dots, m$. Our goal is to write the cycle representation of n -point PT-factor into a form that manifests the factorization into those cycle representations of the m subdiagrams connected to the m -point vertex. Since according to our convention, the $\text{PT}(\boldsymbol{\alpha}_m)$ is read in clockwise direction, we have

$$\text{PT}(\boldsymbol{\alpha}_m) = \langle P_1 P_2 \cdots P_m \rangle \quad (4.8)$$

for the subdiagram inside the blue octagon. We intentionally choose the direction of zig-zag path as clockwise with respect to the considered m -point vertex, so that for this subdiagram, we have

$$\text{PT}(\boldsymbol{\beta}_m) = \langle P_1 P_2 \cdots P_m \rangle \sim (P_1)(P_2) \cdots (P_m). \quad (4.9)$$

⁷It should connect m propagators, but we only sketch eight lines as illustration. The circles with dots inside represent many subdiagrams.

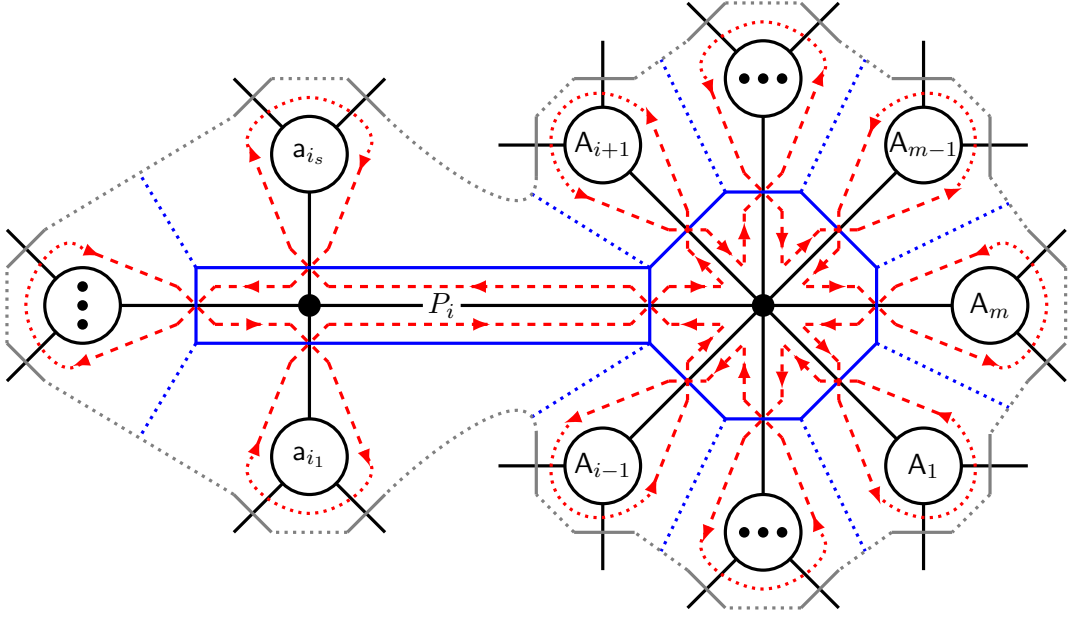


Figure 4: The recursive construction of n -point PT-factor. Black lines represent a general n -point Feynman diagram. Gray lines denotes the dual n -gon. Blue line represent the partial triangulations of n -gon dual to the Feynman diagram, while red dashed lines denote the zig-zag path. The direction of zig-zag path is labeled by arrows in preference of our convention. All dotted lines are abbreviation of their detailed structures that are not explicitly shown in the diagram.

Note that among the $2m$ equivalent cycle representations of $\text{PT}(\beta_m)$, this is the *only* one that allows every P_k appear as a single element in a cycle. Now consider the m subdiagrams in the other side of P_k , denoted as A_1, A_2, \dots, A_m . Since P_k is an external leg of A_k , we know *a priori* that there must be a cycle representation $(P_k)\beta_{A_k}^{\text{cyc-rep}}$ for this subdiagram, where $\beta_{A_k}^{\text{cyc-rep}}$ is to be determined. So when gluing all the m subdiagrams to the one inside the octagon by propagator P_k 's, we obtain the follow factorization form

$$\begin{aligned} \beta^{\text{cyc-rep}} &= (P_1)(P_2)\cdots(P_m) \oplus (P_1)\beta_{A_1}^{\text{cyc-rep}} \oplus \cdots \oplus (P_m)\beta_{A_m}^{\text{cyc-rep}} \\ &= \beta_{A_1}^{\text{cyc-rep}} \beta_{A_2}^{\text{cyc-rep}} \cdots \beta_{A_m}^{\text{cyc-rep}} , \end{aligned} \quad (4.10)$$

namely, it allows a planar separation into m parts. Once the cycle representations of PT-factors for subdiagrams are known, the complete cycle representation is simply a combination of them. Note that the factorization (4.10) is based upon a given vertex. Now we can go into each subdiagram A_i and perform the same construction, until we reach a subdiagram with only one vertex.

A remaining problem is that suppose all the cycle representations of a subdiagram A_i is known, how do we choose the $\beta_{A_i}^{\text{cyc-rep}}$ that is used as the building block of (4.10). According to Fig. 4, the subset A_i and propagator P_i form a $(|A_i| + 1)$ -point subdiagram, connected to the remaining parts via the propagator P_i . In order to connect it with the subdiagram inside octagon, we already constrain the cycle representation of this subdiagram as $(P_i)\beta_{A_i}^{\text{cyc-rep}}$, where (P_i) itself is a cycle. From the definition of equivalent class (2.6),

we know that there are two cycle representations satisfying this condition. One of them can be constructed according to (4.10): suppose the propagator P_i is connected to an $(s + 1)$ -point vertex in subdiagram A_i , marked as black dot in the interior of blue rectangular in Fig. 4. This $(s + 1)$ -point vertex splits the subdiagram A_i into s disjoint sub-subsets a_{i_1} to a_{i_s} via s propagator P_{i_ℓ} with $\ell = 1, \dots, s$. Then following (4.10), we should choose the zig-zag path inside the rectangle in clockwise direction, from which we can obtain a cycle representation satisfying the planar splitting,

$$\beta_{A_{i+1}}^{\text{cyc-rep}} = (P_i)\beta_{A_i}^{\text{cyc-rep}} = (P_i) \beta_{a_{i_1}}^{\text{cyc-rep}} \beta_{a_{i_2}}^{\text{cyc-rep}} \dots \beta_{a_{i_s}}^{\text{cyc-rep}} . \quad (4.11)$$

However, since we have already set the zig-zag path around the octagon to be clockwise, the zig-zag path around the rectangle must be anti-clockwise, and what we should use is the cycle representation other than (4.11) with P_i in a single cycle. Thus we can obtain $(P_i)\beta_{A_i}^{\text{cyc-rep}}$ by acting reversing and cyclic rotation onto (4.11). Moreover, the $\beta_{A_i}^{\text{cyc-rep}}$ obtained this way must be non-planar splitting, namely, at least one cycle of $\beta_{A_i}^{\text{cyc-rep}}$ contains elements from different subsets a_{i_ℓ} . In other words, there must exist at least one cycle that can not be a part of any $\beta_{a_{i_\ell}}^{\text{cyc-rep}}$. To prove this point, it suffices to study the following problem. Given an identity element in the permutation group,

$$\langle P_i, a_1, a_2, \dots, a_i, b_1, b_2, \dots, b_j \rangle , \quad (4.12)$$

which splits into three planar parts $\{P_i\}$, $\{a_1, \dots, a_i\}$ and $\{b_1, \dots, b_j\}$. Let us consider the planar splitting cycle representation $(P_i)\mathbf{a}^{\text{cyc-rep}}\mathbf{b}^{\text{cyc-rep}}$ that maps the identity element (4.12) into another permutation as

$$(P_i) \mathbf{a}^{\text{cyc-rep}} \mathbf{b}^{\text{cyc-rep}} = \begin{pmatrix} P_i & a_1 & a_2 & \dots & a_i & b_1 & b_2 & \dots & b_j \\ \downarrow & \downarrow & \downarrow & \dots & \downarrow & \downarrow & \downarrow & \dots & \downarrow \\ P_i & a'_1 & a'_2 & \dots & a'_i & b'_1 & b'_2 & \dots & b'_j \end{pmatrix} , \quad (4.13)$$

where $\{a'_1, \dots, a'_i\}$ is a permutation of $\{a_1, \dots, a_i\}$ and $\{b'_1, \dots, b'_j\}$ is a permutation of $\{b_1, \dots, b_j\}$. The other cycle representation with (P_i) as a single cycle in equivalent class is thus given by reversing the ordering and dragging P_i to the first position as

$$\begin{pmatrix} P_i & a_1 & a_2 & \dots & a_i & b_1 & \dots & b_{j-1} & b_j \\ \downarrow & \downarrow & \downarrow & \dots & \downarrow & \downarrow & \dots & \downarrow & \downarrow \\ P_i & b'_j & b'_{j-1} & \dots & \dots & \dots & \dots & a'_2 & a'_1 \end{pmatrix} = (P_i)(a_1 b'_j \dots)(\dots) \dots (\dots) . \quad (4.14)$$

Since $b'_j \in \{b_1, \dots, b_j\}$ and $a_1 \in \{a_1, \dots, a_i\}$, it is clear in (4.14) that the legs in two subsets $\{a_1, \dots, a_i\}$, $\{b_1, \dots, b_j\}$ must appear together in at least one cycle in the cycle representation.

To recap, the cycle representation of a Feynman diagram can be written as a simple combination of cycle representations of subdiagrams as presented in (4.10). This leads to a recursive construction of cycle representation from those of lower point Feynman subdiagrams. Crucially, *the cycle representation of subdiagram A_i that used in the complete cycle representation (4.10) should be the one with P_i as a single cycle (P_i) and be non-planar splitting with respect to its vertex connected to P_i .* Then we can work out

the permutation from cycle representation and eventually the PT-factor $\text{PT}(\beta)$. Note that, it is possible to start the recursive construction from any vertex of a Feynman diagram, and different choice leads to different cycle representation but they are all in the same equivalent class. We will show in Appendix A that different planar splittings characterize the shapes of the associahedron boundaries.

4.3 Examples

Let us now present some nontrivial examples to illustrate the recursive construction of cycle representation. First we consider the three point diagram. The cubic vertex splits diagram into three subdiagrams, each one is trivially a single external leg. This is also true for the diagrams with only a single vertex. So following (4.10), we get

$$\begin{array}{c} 2 \\ \diagdown \\ \bullet \\ \diagup \\ 1 \end{array} \begin{array}{c} 3 \\ \text{---} \\ \bullet \end{array} \iff \beta^{\text{cyc-rep}} = (1)(2)(3) \quad , \quad \begin{array}{c} 3 \cdots \cdots \\ \diagdown \\ \bullet \\ \diagup \\ 1 \end{array} \begin{array}{c} 2 \text{---} \\ \text{---} \\ \bullet \end{array} \begin{array}{c} n \\ \text{---} \\ \bullet \end{array} \iff \beta^{\text{cyc-rep}} = (1)(2)(3) \dots (n) . \quad (4.15)$$

Note that $(12)(3)$ is in the same equivalent class of $(1)(2)(3)$ for this three point diagram. When it appears as a subdiagram, one leg becomes an internal line P , namely

$$\begin{array}{c} a_2 \\ \diagdown \\ \bullet \\ \diagup \\ a_1 \end{array} \begin{array}{c} P \\ \text{---} \\ \bullet \end{array} \begin{array}{c} \text{---} \\ \text{---} \\ \bullet \end{array} . \quad (4.16)$$

In this case, we should use the non-planar splitting cycle representation $(a_1 a_2)(P)$ instead of $(a_1)(a_2)(P)$. To see this, let us proceed to a four point Feynman diagram as shown below. If we start from the vertex marked by red dot, the diagram splits to three subdiagrams, two of which are single external legs and one is three point subdiagram. The non-planar splitting for three point subdiagram appears as $(12)(P_{12})$, so according to (4.10), the recursive procedure is described as follows,

$$\begin{array}{c} 2 \\ \diagdown \\ \bullet \\ \diagup \\ 1 \end{array} \begin{array}{c} \text{---} \\ \text{---} \\ \bullet \end{array} \begin{array}{c} 3 \\ \diagdown \\ \bullet \\ \diagup \\ 4 \end{array} \longrightarrow \begin{array}{c} (1)(2)(P_{12}) \\ \downarrow \\ (12)(P_{12}) \\ \swarrow \\ \begin{array}{c} 2 \\ \diagdown \\ \bullet \\ \diagup \\ 1 \end{array} \begin{array}{c} \text{---} \\ \text{---} \\ \bullet \end{array} P_{12} \begin{array}{c} 3 \\ \diagdown \\ \bullet \\ \diagup \\ 4 \end{array} \\ \nearrow \\ (P_{34})(3)(4) \end{array} \implies \beta^{\text{cyc-rep}} = (12)(3)(4) . \quad (4.17)$$

From above results, we can recursively compute the cycle representation of $\text{PT}(\beta)$ for five point CHY-integrand. Here we present an example as follows,

$$\begin{array}{c} 2 \\ \diagdown \\ \bullet \\ \diagup \\ 1 \end{array} \begin{array}{c} \text{---} \\ \text{---} \\ \bullet \end{array} \begin{array}{c} 3 \\ \text{---} \\ \bullet \\ \text{---} \\ \bullet \end{array} \begin{array}{c} 4 \\ \diagdown \\ \bullet \\ \diagup \\ 5 \end{array} , \quad (4.18)$$

and construct the cycle representation starting from two different vertices respectively. If we start from vertex V_1 , then the diagram is split to three parts: the external leg 4, 5 and a four point subdiagram. As mentioned above, $(12)(3)(P_{123})$ is a planar splitting cycle representation with respect to V_2 , and we should take the non-planar splitting one in the equivalent class, namely, $(132)(P_{123})$, to form the complete cycle representation, which is obtained from $(12)(3)(P)$ by acting the reversing permutation $(13)(2)$, namely, $[(12)(3)] \cdot [(13)(2)] = (132)$. Hence, the final result is $(132)(4)(5)$.

Alternatively, we can start from vertex V_2 . Then the diagram is split to another three parts, two of which are three point subdiagrams with non-planar splitting cycle representation $(12)(P_{12})$ and $(45)(P_{45})$, while the other is the single external leg 3. Connecting them via the vertex $(P_{12})(P_3)(P_{45})$, we obtain $(12)(3)(45)$. We see that different splitting of diagram leads to different cycle representations. However, all of them are in the same equivalent class. In fact, both $(132)(4)(5)$ and $(12)(3)(45)$ lead to the PT-factor $\text{PT}(\beta) = \langle 12453 \rangle$.

Next, we give a seven point example. The Feynman diagram is shown below, together with the resultant cycle representations when we carry out the recursive construction at different vertices,

(V_1)	$\beta = (1)(2)(347)(5)(6)$	
(V_2)	$\beta = (12)(3)(467)(5)$	
(V_3)	$\beta = (132)(4)(576)$	(4.19)
(V_4)	$\beta = (143)(2)(56)(7)$	
(V_5)	$\beta = (1)(2)(347)(5)(6)$	

Some brief explanation is in order. For the vertex V_4 , the planar splitting cycle representation is $(P)(56)(7)$, while its non-planar splitting one is $[(7)(56)] \cdot [(75)(6)] = (576)$. The former can be used in the recursive construction starting from vertex V_4 , while the latter can be used in the recursive construction starting from vertex V_3 . Similarly, for the vertex V_3 , the planar splitting cycle representation is $(P)(4)(576)$, while the non-planar splitting one is $[(4)(576)] \cdot [(47)(56)] = (467)(5)$. The latter can be used in the recursive construction starting from vertex V_2 .

This recursive construction can be easily taken to higher points, and we have run extensive checking up to eight point diagrams.

5 Relations between different PT-factors

After clarifying the relations between permutations of PT-factors and the Feynman diagrams, we move on to the relations between different PT-factors in the language of permutation and cycle representation. This topic has been discussed from the *associahedron* point of view [31] and before proceeding let us briefly review their result. The major conclusion is that, the canonical form of an $(n - 3)$ -dimensional associahedron is the n -particle tree-level amplitude of bi-adjoint scalar theory with identical ordering. A consequence is that, the codimension d faces of an associahedron are in one-to-one correspondence with the partial triangulations with d diagonals, while the partial triangulations are dual to cuts on planar cubic



Figure 5: The associahedron for four point amplitudes and PT-factors.

diagrams with each diagonal corresponding to a cut. Hence the faces of the associahedron are dual to the singularities of cubic scalar amplitude. In this sense, PT-factors can also be related to corresponding faces of associahedron. For instance, a three point amplitude is dual to a triangle, allowing only one trivial triangulation. Thus the corresponding associahedron is just a zero dimensional point, on which sits the only independent PT-factor $\text{PT}(\boldsymbol{\beta}) = \langle 123 \rangle$. A four point amplitude is dual to a box, while the associahedron formed by its (partial) triangulations is a one dimensional line as shown in Fig. 5. The vertices correspond to all complete triangulations of the box, while the edge corresponds to partial triangulations. The edge is related to $\text{PT}(\boldsymbol{\beta}) = \langle 1234 \rangle$ with amplitude $\frac{1}{s_{12}} + \frac{1}{s_{23}}$, while the two ending vertices are related to $\text{PT}(\boldsymbol{\beta}) = \langle 1243 \rangle$ and $\langle 1324 \rangle$ respectively with amplitude $\frac{1}{s_{12}}$ and $\frac{1}{s_{23}}$. The relations between different PT-factors are manifest in this geometric picture.

A five point amplitude is dual to a pentagon, and the associahedron constructed from all its (partial) triangulations is also a pentagon, as shown in Fig. 6, where the thick black lines form the associahedron and the blue line is the triangulations of pentagon. The face corresponds to $\langle 12345 \rangle$, while the edges correspond to $\langle 12543 \rangle$, $\langle 12354 \rangle$, $\langle 13245 \rangle$, $\langle 14325 \rangle$, $\langle 12435 \rangle$, and the vertices correspond to $\langle 12453 \rangle$, $\langle 13254 \rangle$, $\langle 14235 \rangle$, $\langle 13425 \rangle$, $\langle 12534 \rangle$. The PT-factor of each vertex evaluates to a single Feynman diagram. An edge connects two vertices, which means that the PT-factor of the edge evaluates to two Feynman diagrams. Two edges share a common point, which means that there is common Feynman diagram shared by them. The face contains five vertices, such that its PT-factor evaluates to five Feynman diagrams. Therefore the relation among different PT-factors is obvious in the diagram. For higher point amplitude, the associahedron would be much more complicated geometric objects, however the correspondence is similar.

5.1 Relation analysis via cycle representation

From the n -gon picture, we see that by adding one more triangulation line (i.e., fix one more propagator), we get the immediate child amplitude. In contrary, by removing one triangulation line (i.e., unfix a propagator),

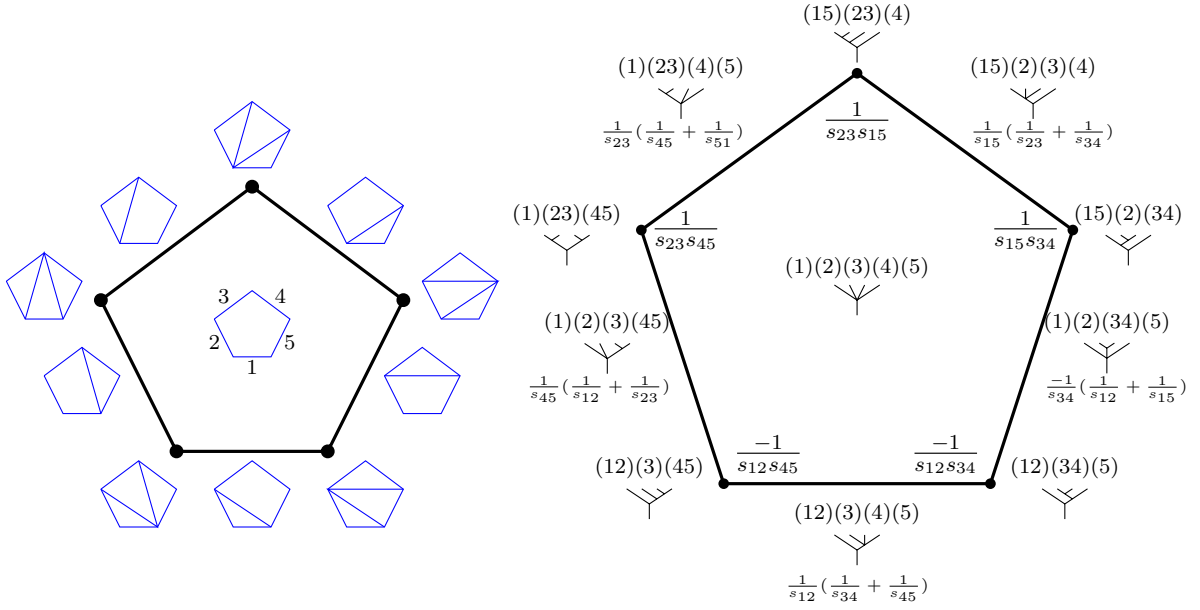
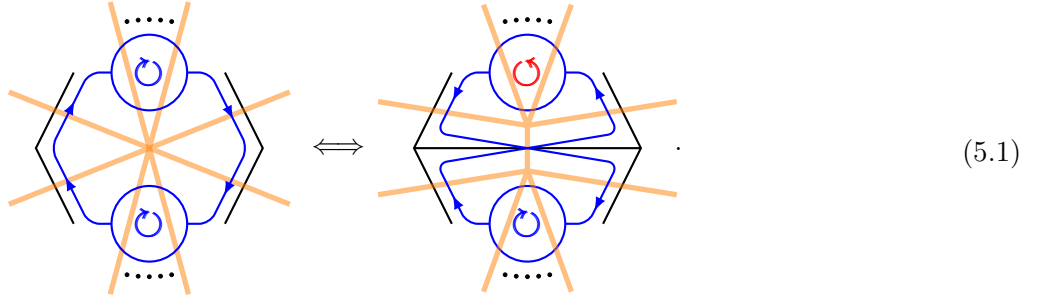


Figure 6: The associahedron for five point amplitudes and the PT-factors.

we recover the mother amplitude. In terms of zig-zag path, we have the following picture,



The extra triangulation separates the n -gon into two subpolygons. Notably, in one of them we need to reverse the ordering. In this section, we study how the above picture is realized by good cycle representations, namely, how to merge or split certain parts in good cycle representations to fix or unfix a propagator.

We start with the general discussion. The left hand side of Eq. (5.1) indicates that there exists a good cycle representation with the form

$$\beta = \beta_{\text{lower}}\beta_{\text{upper}} = \underbrace{(\dots)|(\dots)(\dots)|\dots(\dots)}_{\text{lower}} \Big| \underbrace{(\dots)|(\dots)(\dots)|\dots(\dots)}_{\text{upper}}, \quad (5.2)$$

where subscripts lower and upper denote the external legs below and above the extra triangulation line in (5.1). This cycle representation can either be a V-type or P-type one. Suppose the upper set consists of

$$\text{upper} = \{i, i + 1 \dots j\}, \quad (5.3)$$

then the reversing process of (5.1) can be realized by

$$\beta_{\text{upper}}^{\text{reversed}} = \beta_{\text{upper}} \beta_r, \quad (5.4)$$

where β_r simply flips the ordering $\beta_r|i, i+1 \dots j\rangle = |j \dots i+1, i\rangle$. Similar to Eq. (2.5), β_r has the cycle representation

$$\beta_r = \begin{cases} (ij)(i+1, j-1) \dots \left(\frac{i+j-1}{2}, \frac{i+j+1}{2}\right) & j-i = \text{odd} \\ (ij)(i+1, j-1) \dots \left(\frac{i+j-2}{2}, \frac{i+j+2}{2}\right) \left(\frac{i+j}{2}\right) & j-i = \text{even} \end{cases}. \quad (5.5)$$

Therefore, the process of (5.1) can be realized in an algebraic way as⁸

$$\beta_{\text{lower}} \beta_{\text{upper}} \iff \beta_{\text{lower}} \beta_{\text{upper}} \beta_r. \quad (5.6)$$

If the propagator manifested in (5.2) is an *overall* one, then the above process gives the immediate mother amplitude that has the original amplitude as a part. *Otherwise*, the above process gives the immediate child amplitude that contains this propagator as an overall factor, and is a part of the original amplitude.

Next, we use the example given in (3.3) with cycle representations (3.4) to demonstrate our idea,

$$\text{PT}(\beta) = \langle 12846573 \rangle \implies \frac{1}{s_{12}s_{56}s_{8123}} \left(\frac{1}{s_{812}} + \frac{1}{s_{123}} \right) \left(\frac{1}{s_{456}} + \frac{1}{s_{567}} \right). \quad (5.7)$$

We first consider its immediate child amplitudes by fixing the poles s_{812} , s_{123} , s_{456} and s_{567} one by one.

Fix the pole s_{812} : To achieve this goal, we need to use the good cycle representations that manifest the separation $\{8, 1, 2\}$ and $\{3, 4, 5, 6, 7\}$. In (3.4), only $(12)(3)(47)(5)(6)(8)$ and $(128)(3467)(5)$ satisfy the condition. We can achieve the child amplitude by using either one. Starting with $(12)(3)(47)(5)(6)(8)$, we split all cycles into two parts according to the pole, namely, $(8)(12)|(3)(47)(5)(6)$. Now we can keep one part invariant and perform the prescription (5.4) to the other. For example, we keep the part $(8)(12)$, such that for another part we should do the following manipulation as

$$[(3)(47)(5)(6)] \cdot [(37)(46)(5)] = (3467)(5), \quad (5.8)$$

where $(37)(46)(5)$ is the reversing permutation β_r obtained from (5.5). Putting the two parts together, we get the cycle representation $(8)(12)(3467)(5)$, which corresponds to the PT-factor $\text{PT}(\beta) = \langle 12837564 \rangle$. It indeed gives the desired child amplitude,

$$\text{PT}(\beta) = \langle 12837564 \rangle \implies \frac{1}{s_{12}s_{56}s_{8123}} \left(\frac{1}{s_{812}} \right) \left(\frac{1}{s_{456}} + \frac{1}{s_{567}} \right). \quad (5.9)$$

Alternatively, we keep the part $(3)(47)(5)(6)$ intact and act the prescription (5.4) onto the part $(8)(12)$,

$$[(8)(12)] \cdot [(82)(1)] = (812). \quad (5.10)$$

⁸Equivalently, we can reverse the lower part. The result will only differ by an overall reversing.

Putting them together, we get another cycle representation $(812)(3)(47)(5)(6)$, corresponding to the same PT-factor as (5.9). If we use the other cycle representation $(128)[(3467)(5)$, we get the same result,

$$\begin{aligned} [(128)] \cdot [(82)(1)](3476)(5) &= (8)(12)(3467)(5) , \\ (128)[(3467)(5)] \cdot [(37)(46)(5)] &= (128)(3)(47)(5)(6) . \end{aligned} \quad (5.11)$$

Fix the pole s_{123} : For this case, the cycle representations $(12)(3)(47)(5)(6)(8)$ and $(132)(4875)(6)$ from (3.4) can be used. By similar manipulations, we get

$$(12)(3)(47)(5)(6)(8) \implies \begin{cases} [(12)(3)] \cdot [(13)(2)](47)(5)(6)(8) = (132)(47)(5)(6)(8) \\ (12)(3)[(47)(5)(6)(8)] \cdot [(48)(57)(6)] = (12)(3)(4875)(6) \end{cases} , \quad (5.12a)$$

$$(132)(4875)(6) \implies \begin{cases} (132) \cdot [(13)(2)](4875)(6) = (12)(3)(4875)(6) \\ (132)[(4875)(6)] \cdot [(48)(57)(6)] = (132)(47)(5)(6)(8) \end{cases} . \quad (5.12b)$$

Both results correspond to the PT-factor $\text{PT}(\boldsymbol{\beta}) = \langle 12756483 \rangle$, which is evaluated to

$$\frac{1}{s_{12}s_{56}s_{8123}} \left(\frac{1}{s_{123}} \right) \left(\frac{1}{s_{456}} + \frac{1}{s_{567}} \right) . \quad (5.13)$$

Fix the pole s_{456} : For this case, the cycle representations $(1)(2)(38)(4)(56)(7)$ and $(1)(2378)(456)$ from (3.4) can be used. By similar manipulations we get

$$(1)(2)(38)(4)(56)(7) \implies \begin{cases} (1)(2)(38)(7)[(4)(56)] \cdot [(46)(5)] = (1)(2)(38)(7)(456) \\ [(1)(2)(38)(7)] \cdot [(73)(82)(1)](4)(56) = (1)(2378)(4)(56) \end{cases} , \quad (5.14a)$$

$$(1)(2378)(456) \implies \begin{cases} (1)(2378)[(456)] \cdot [(46)(5)] = (1)(2378)(4)(56) \\ [(1)(2378)] \cdot [(73)(82)(1)](456) = (1)(2)(38)(7)(456) \end{cases} . \quad (5.14b)$$

Both results correspond to the PT-factor $\text{PT}(\boldsymbol{\beta}) = \langle 12856473 \rangle$, which is evaluated to

$$\frac{1}{s_{12}s_{56}s_{8123}} \left(\frac{1}{s_{123}} + \frac{1}{s_{812}} \right) \left(\frac{1}{s_{456}} \right) . \quad (5.15)$$

Fix the pole s_{567} : For this case, the cycle representations $(1)(2)(38)(4)(56)(7)$ and $(1843)(2)(576)$ from (3.4) can be used. By similar manipulations we get

$$(1)(2)(38)(4)(56)(7) \implies \begin{cases} (1)(2)(38)(4)[(56)(7)] \cdot [(57)(6)] = (1)(2)(38)(4)(576) \\ [(1)(2)(38)(4)] \cdot [(84)(13)(2)](56)(7) = (8431)(2)(56)(7) \end{cases} , \quad (5.16a)$$

$$(1843)(2)(576) \implies \begin{cases} (1843)(2)[(576)] \cdot [(57)(6)] = (1843)(2)(56)(7) \\ [(1843)(2)] \cdot [(84)(13)(2)](576) = (1)(2)(38)(4)(576) \end{cases} . \quad (5.16b)$$

Both results correspond to the PT-factor $\text{PT}(\boldsymbol{\beta}) = \langle 12847563 \rangle$, which is evaluated to

$$\frac{1}{s_{12}s_{56}s_{1238}} \left(\frac{1}{s_{123}} + \frac{1}{s_{812}} \right) \left(\frac{1}{s_{567}} \right) . \quad (5.17)$$

After showing how to get the child amplitudes, we now discuss the case of mother amplitudes. This happens when we perform the prescription (5.4) to a separation that manifests an *overall* propagator. For the case (5.7), there are three common poles s_{12} , s_{56} and s_{8123} . Relaxing any one of them, we can get a mother amplitude. The procedure is similar to the above discussion, and we again do it one by one.

Unfix the pole s_{12} : For this case, the following two cycle representations (1)(2)(38)(4)(56)(7) and (12)(3)(47)(5)(6)(8) manifest the pole s_{12} . If we take (1)(2)(38)(4)(56)(7), we have the following calculation according to (5.4),

$$(1)(2)(38)(4)(56)(7) \implies \begin{cases} [(1)(2)] \cdot [(12)](38)(4)(56)(7) = (12)(38)(4)(56)(7) \\ (1)(2)[(38)(4)(56)(7)] \cdot [(38)(47)(56)] = (1)(2)(3)(47)(5)(6)(8) \end{cases}, \quad (5.18a)$$

$$(12)(3)(47)(5)(6)(8) \implies \begin{cases} [(12)] \cdot [(12)](3)(47)(5)(6)(8) = (1)(2)(3)(47)(5)(6)(8) \\ (12)[(3)(47)(5)(6)(8)] \cdot [(38)(47)(56)] = (12)(38)(4)(56)(7) \end{cases}, \quad (5.18b)$$

which correspond to $\text{PT}(\beta) = \langle 12375648 \rangle$. It gives ten terms, among which four are just (5.7).

Unfix the pole s_{56} : For this case, the cycle representations (1)(2)(38)(4)(56)(7) and (12)(3)(47)(5)(6)(8) manifest the pole s_{56} . We have the following calculation according to (5.4),

$$(1)(2)(38)(4)(56)(7) \implies \begin{cases} [(56)] \cdot [(56)](1)(2)(38)(4)(7) = (1)(2)(38)(4)(5)(6)(7) \\ (56)[(1)(2)(38)(4)(7)] \cdot [(47)(38)(12)] = (56)(12)(3)(8)(47) \end{cases}, \quad (5.19a)$$

$$(12)(3)(47)(5)(6)(8) \implies \begin{cases} [(5)(6)] \cdot [(56)](12)(3)(47)(8) = (12)(3)(47)(56)(8) \\ (5)(6)[(12)(3)(47)(8)] \cdot [(47)(38)(12)] = (5)(6)(1)(2)(4)(7)(38) \end{cases}. \quad (5.19b)$$

One can check that they correspond to $\text{PT}(\beta) = \langle 12845673 \rangle$. It also gives ten terms, among which four are just (5.7).

Unfix the pole s_{8123} : For this case, we have two good cycle representations (1)(2)(38)(4)(56)(7) and (12)(3)(47)(5)(6)(8) that manifest the pole s_{8123} . We have the following calculation according to (5.4),

$$(1)(2)(38)(4)(56)(7) \implies \begin{cases} [(1)(2)(38)] \cdot [(12)(38)](4)(56)(7) = (12)(3)(8)(4)(56)(7) \\ (1)(2)(38)[(4)(56)(7)] \cdot [(47)(56)] = (1)(2)(38)(47)(5)(6) \end{cases}, \quad (5.20a)$$

$$(12)(3)(47)(5)(6)(8) \implies \begin{cases} [(12)(3)(8)] \cdot [(12)(38)](47)(5)(6) = (1)(2)(38)(47)(5)(6) \\ (12)(3)(8)[(47)(5)(6)] \cdot [(47)(56)] \rightarrow (12)(3)(8)(4)(56)(7) \end{cases}, \quad (5.20b)$$

which correspond to $\text{PT}(\beta) = \langle 12875643 \rangle$. It gives 14 terms, among which four are just (5.7).

5.2 Relation analysis via cross-ratio factor

We can also study the relations of PT-factor from another approach. As we have already known, the relations between different PT-factors can be seen as selecting terms corresponding to specific pole structures in the evaluated results. For instance, $\langle 1234 \rangle \langle 1234 \rangle$ evaluates to $\frac{1}{s_{12}} + \frac{1}{s_{23}}$ while $\langle 1234 \rangle \langle 1243 \rangle$ evaluates to $\frac{1}{s_{12}}$. It

means that, by selecting terms with pole $\frac{1}{s_{12}}$ in $\langle 1234 \rangle \langle 1234 \rangle$, we can reproduce the result of $\langle 1234 \rangle \langle 1243 \rangle$. To achieve this goal at the CHY-integrand level, we can use the cross-ratio factor given in paper [38], which we will call it the *selecting factor*

$$f^{\text{select}}[a, b, c, d] := \frac{[ab][cd]}{[ac][bd]} \quad , \quad [ab] := \sigma_{ab} . \quad (5.21)$$

To pick up the Feynman diagrams with a pole $\frac{1}{s_A}$ from a given CHY-integral result, where A follows a certain color ordering, we propose to multiply the CHY-integrand with a selecting factor $f^{\text{select}}[\bar{A}_{-1}, A_1, A_{-1}, \bar{A}_1]$, where A_1, A_{-1} are the first and last elements of the subset A respectively, and \bar{A} is the complement subset of A , i.e., in order to pick up terms with pole $\frac{1}{s_A}$, the arguments b, c in the selecting factor should be the two ending legs in the set A , while the arguments a, d are the nearby two legs of b, c outside the set A respectively. As an illustration, let us consider the above mentioned PT-factors $\langle 1234 \rangle$ and $\langle 1243 \rangle$. We want to select terms with $\frac{1}{s_{12}}$ pole in the evaluated result of $\langle 1234 \rangle \langle 1234 \rangle$, which means that we need to take the selecting factor $f^{\text{select}}[4, 1, 2, 3]$,

$$\langle 1234 \rangle f^{\text{select}}[4, 1, 2, 3] = \frac{1}{\sigma_{12}\sigma_{23}\sigma_{34}\sigma_{41}} \frac{\sigma_{41}\sigma_{23}}{\sigma_{42}\sigma_{13}} = - \langle 1243 \rangle . \quad (5.22)$$

It indeed produces the PT-factor $\langle 1243 \rangle$, despite of the overall sign.

There is a subtlety in the choice of the selecting factor. The bi-adjoint scalar theory has two color orderings, given by $\text{PT}(\boldsymbol{\alpha})$ and $\text{PT}(\boldsymbol{\beta})$. We should choose A to follow one of the orderings. If $\boldsymbol{\alpha} = \boldsymbol{\beta}$, there is no ambiguity in defining the selecting factor, which is the situation discussed in [38]. However if $\boldsymbol{\alpha} \neq \boldsymbol{\beta}$, the multiplication

$$\text{PT}(\boldsymbol{\alpha}) \times \text{PT}(\boldsymbol{\beta}) \times f^{\text{select}}[\bar{A}_{-1}, A_1, A_{-1}, \bar{A}_1] \quad (5.23)$$

has two choices for a given set A . The arguments of f^{select} depend on the color ordering of legs, and we have two color orderings to rely on. It can be shown that although we would get two different selecting factors, the resulting CHY-integrands are equivalent in the sense that the difference of two CHY-integrands evaluates to zero. We note that this happens only when $\frac{1}{s_A}$ is indeed a physical pole of the integrated result of $\text{PT}(\boldsymbol{\alpha}) \times \text{PT}(\boldsymbol{\beta})$, but not an *overall* one.

Now let us present a brief explanation about why the selecting factor f^{select} is able to pick up terms with specific poles. It is known that from [14–16], the order of pole $\frac{1}{s_A}$ in the evaluated result is characterized by the *pole index*

$$\chi[A] = \mathbb{L}[A] - 2(|A| - 1) , \quad (5.24)$$

where $\mathbb{L}[A]$ is the linking number of subset A , and $|A|$ is the length of subset A .⁹ If $\chi[A] < 0$, there is no s_A pole, while if $\chi[A] \geq 0$, the pole would appear in the result as $\frac{1}{s_A^{\chi+1}}$. For CHY-integrands with two PT-factors, we only have simple poles, namely, $\chi[A] \leq 0$ for any subset A . With this in mind, let us take

⁹The linking number $\mathbb{L}[A]$ can be read out from the so-called *4-regular* diagrams, which is discussed in details in [14–16].

a further look on the selecting factor f^{select} , assuming that $\frac{1}{s_A}$ is not an overall pole. The combinations in both the numerator and denominator of f^{select} represent lines connecting elements in subset A and its complement \bar{A} , so that f^{select} will not change the linking number of A itself: after multiplying f^{select} , we still have $\chi[A] = 0$ and the pole $\frac{1}{s_A}$ remains unchanged. Now suppose there is another pole $\frac{1}{s_B}$, where B has nonempty overlap with both A and \bar{A} , then it will be removed by f^{select} . The reason is that in the denominator of PT-factor there are $[A_{-1}\bar{A}_1]$ and $[\bar{A}_{-1}A_1]$, while in the numerator of the selecting factor there are $[A_{-1}\bar{A}_1]$ and $[\bar{A}_{-1}A_1]$, which at least reduces the linking number of subset B by one, such that $\chi[B]$ is reduced from 0 to -1 . Thus all the poles that are not compatible with $\frac{1}{s_A}$ are removed. Finally, we need to show that the terms with $\frac{1}{s_A}$ are not altered by the selecting factor, namely, we should confirm that in a term with pole $\frac{1}{s_A}$, f^{select} do not change the pole indices of all the other poles. By the compatibility condition, these poles should either be a subset of A or a subset of \bar{A} . For the four factors $[\bar{A}_{-1}A_1]$, $[A_{-1}\bar{A}_1]$, $[\bar{A}_{-1}A_{-1}]$ and $[A_1\bar{A}_1]$ in f^{select} , each one contains an element from subset A and another from \bar{A} , so that none of them contributes to the linking number of either A or \bar{A} .

In general, when using f^{select} to pick up a pole $\frac{1}{s_A}$, we will encounter three situations. In the first situation, the original theory does not contain such a pole. Then multiplying the selecting factor does not make any sense. For instance, the CHY-integrand $\langle 123456 \rangle \langle 124563 \rangle$ evaluates to

$$\langle 123456 \rangle \times \langle 124563 \rangle \rightarrow \frac{1}{s_{12}s_{123}} \left(\frac{1}{s_{45}} + \frac{1}{s_{56}} \right), \quad (5.25)$$

which does not contain the pole $\frac{1}{s_{34}}$. If we insist to take the selecting factor $f^{\text{select}}[2, 3, 4, 5]$ following the color ordering of the first PT-factor, we get

$$\left(\langle 123456 \rangle f^{\text{select}}[2, 3, 4, 5] \right) \times \langle 124563 \rangle \rightarrow -\frac{1}{s_{56}s_{124}} \left(\frac{1}{s_{12}} + \frac{1}{s_{56}} \right), \quad (5.26)$$

which is a completely irrelevant answer.

In the second situation, the pole $\frac{1}{s_A}$ we pick is overall to all the terms. By multiplying the selecting factor, we produce the mother amplitude, obtained by pinching the propagator $\frac{1}{s_A}$ in the Feynman diagram. For example, there are two overall poles $\frac{1}{s_{12}}$ and $\frac{1}{s_{123}}$ in (5.25). If we follow the color ordering of the first PT-factor, and multiply $f^{\text{select}}[6, 1, 2, 3]$ that corresponds to $\frac{1}{s_{12}}$, we get

$$\left(\langle 123456 \rangle f^{\text{select}}[6, 1, 2, 3] \right) \times \langle 124563 \rangle \rightarrow \frac{1}{s_{12}s_{123}} \left(\frac{1}{s_{45}} + \frac{1}{s_{56}} \right) + \frac{1}{s_{13}s_{123}} \left(\frac{1}{s_{45}} + \frac{1}{s_{56}} \right), \quad (5.27)$$

which is a mother amplitude with additional terms produced. Similarly, if we follow the color ordering of the second PT-factor, and multiply $f^{\text{select}}[3, 1, 2, 4]$ that corresponds to $\frac{1}{s_{12}}$, we get

$$\langle 123456 \rangle \times \left(\langle 124563 \rangle f^{\text{select}}[3, 1, 2, 4] \right) \rightarrow \frac{1}{s_{12}s_{123}} \left(\frac{1}{s_{45}} + \frac{1}{s_{56}} \right) + \frac{1}{s_{23}s_{123}} \left(\frac{1}{s_{45}} + \frac{1}{s_{56}} \right), \quad (5.28)$$

which is another mother amplitude with different additional terms produced. Similar calculation can be done for the overall pole s_{123} and the two different mother amplitudes are given by

$$\begin{aligned} \langle (123456) f^{\text{select}}[6, 1, 3, 4] \rangle \times \langle 124563 \rangle &\rightarrow \frac{1}{s_{12}s_{123}} \left(\frac{1}{s_{45}} + \frac{1}{s_{56}} \right) + \frac{1}{s_{12}s_{124}} \left(\frac{1}{s_{36}} + \frac{1}{s_{56}} \right) + \frac{1}{s_{12}s_{36}s_{45}}, \\ \langle 123456 \rangle \times \langle (124563) f^{\text{select}}[6, 3, 2, 4] \rangle &\rightarrow \frac{1}{s_{12}s_{123}} \left(\frac{1}{s_{45}} + \frac{1}{s_{56}} \right) + \frac{1}{s_{12}s_{126}} \left(\frac{1}{s_{34}} + \frac{1}{s_{45}} \right) + \frac{1}{s_{12}s_{34}s_{56}}, \end{aligned}$$

indicating that (5.25) can be part of the mother amplitudes with different color orderings.

In the third situation, the pole we pick is physical but an overall one, thus multiplying the selecting factor we get the immediate child amplitude. This is the case we have considered in detail in the beginning of this subsection. Consider an eight point CHY-integrand with $\text{PT}(\boldsymbol{\alpha}) = \langle 12345678 \rangle$ and $\text{PT}(\boldsymbol{\beta}) = \langle 12348765 \rangle$. The amplitude is

$$\begin{aligned} \text{PT}(\boldsymbol{\alpha})\text{PT}(\boldsymbol{\beta}) &\rightarrow \frac{1}{s_{1234}} \left(\frac{1}{s_{12}s_{34}} + \frac{1}{s_{12}s_{123}} + \frac{1}{s_{23}s_{123}} + \frac{1}{s_{23}s_{234}} + \frac{1}{s_{34}s_{234}} \right) \\ &\quad \times \left(\frac{1}{s_{56}s_{78}} + \frac{1}{s_{56}s_{567}} + \frac{1}{s_{67}s_{567}} + \frac{1}{s_{67}s_{678}} + \frac{1}{s_{78}s_{678}} \right) \\ &= \frac{1}{s_{1234}} \left(\begin{array}{c} 3 \quad 4 \\ \diagdown \quad \diagup \\ P_{1234} \\ \diagup \quad \diagdown \\ 2 \quad 1 \end{array} \right) \left(\begin{array}{c} 5 \quad 6 \\ \diagdown \quad \diagup \\ P_{5678} \\ \diagup \quad \diagdown \\ 8 \quad 7 \end{array} \right), \end{aligned} \quad (5.29)$$

where we used the five point vertices to represent the terms in two parentheses. For instance, if we want to pick up terms with pole $\frac{1}{s_{78}}$, either $f^{\text{select}}[6, 7, 8, 1]$ following the color ordering of $\text{PT}(\boldsymbol{\alpha})$ or $f^{\text{select}}[4, 8, 7, 6]$ following the color ordering of $\text{PT}(\boldsymbol{\beta})$ can do the job. Indeed, by direct computation, we confirm that

$$\left. \begin{aligned} & \left(\text{PT}(\boldsymbol{\alpha}) f^{\text{select}}[6, 7, 8, 1] \right) \times \text{PT}(\boldsymbol{\beta}) \\ & \text{PT}(\boldsymbol{\alpha}) \times \left(\text{PT}(\boldsymbol{\beta}) f^{\text{select}}[4, 8, 7, 6] \right) \end{aligned} \right\} \rightarrow \frac{1}{s_{1234}} \times \frac{1}{s_{78}} \left(\frac{1}{s_{56}} + \frac{1}{s_{678}} \right) \times \left(\begin{array}{c} 3 \quad 4 \\ \diagdown \quad \diagup \\ P_{1234} \\ \diagup \quad \diagdown \\ 2 \quad 1 \end{array} \right). \quad (5.30)$$

In fact, we can multiply more than one selecting factors to pick up terms with several specific poles. For example, if we want to pick up terms with pole $\frac{1}{s_{78} s_{678}}$, we can start from the result (5.30) and take the selecting factor $f^{\text{select}}[5, 6, 8, 1]$ following the color ordering of $\text{PT}(\boldsymbol{\alpha})$ in the second row of (5.30), or $f^{\text{select}}[4, 8, 6, 5]$ following the color ordering of $\text{PT}(\boldsymbol{\beta})$ in the first row of (5.30). It leads to four possible multiplications, and by direct computation, they produce the same result as

$$\left. \begin{aligned} & \text{PT}(\boldsymbol{\alpha}) f^{\text{select}}[6, 7, 8, 1] f^{\text{select}}[5, 6, 8, 1] \times \text{PT}(\boldsymbol{\beta}) \\ & \text{PT}(\boldsymbol{\alpha}) f^{\text{select}}[6, 7, 8, 1] \times \left(\text{PT}(\boldsymbol{\beta}) f^{\text{select}}[4, 8, 6, 5] \right) \\ & \left(\text{PT}(\boldsymbol{\alpha}) f^{\text{select}}[5, 6, 8, 1] \right) \times \left(\text{PT}(\boldsymbol{\beta}) f^{\text{select}}[4, 8, 7, 6] \right) \\ & \text{PT}(\boldsymbol{\alpha}) \times \left(\text{PT}(\boldsymbol{\beta}) f^{\text{select}}[4, 8, 7, 6] f^{\text{select}}[4, 8, 6, 5] \right) \end{aligned} \right\} \rightarrow \frac{1}{s_{1234}} \times \frac{1}{s_{78}s_{678}} \times \left(\begin{array}{c} 3 \quad 4 \\ \diagdown \quad \diagup \\ P_{1234} \\ \diagup \quad \diagdown \\ 2 \quad 1 \end{array} \right). \quad (5.31)$$

We note that the first and last of them do not end up directly with pure PT-factors. Nontrivial identities are required to further reduce the results. Thus, multiplying the selecting factor is a little bit broader than the situation discussed in the previous subsection.

We can further pick up terms with, say, $\frac{1}{s_{12}}$ pole, from the previous result. It can be checked that the following eight multiplications of selecting factors

$$\begin{aligned}
& (\text{PT}(\boldsymbol{\alpha})f[6, 7, 8, 1]f[5, 6, 8, 1]f[8, 1, 2, 3]) \times \text{PT}(\boldsymbol{\beta}) && (\text{PT}(\boldsymbol{\alpha})f[6, 7, 8, 1]f[5, 6, 8, 1]) \times (\text{PT}(\boldsymbol{\beta})f[5, 1, 2, 3]) \\
& (\text{PT}(\boldsymbol{\alpha})f[6, 7, 8, 1]f[8, 1, 2, 3]) \times (\text{PT}(\boldsymbol{\beta})f[4, 8, 6, 5]) && (\text{PT}(\boldsymbol{\alpha})f[6, 7, 8, 1]) \times (\text{PT}(\boldsymbol{\beta})f[4, 8, 6, 5]f[5, 1, 2, 3]) \\
& (\text{PT}(\boldsymbol{\alpha})f[5, 6, 8, 1]f[8, 1, 2, 3]) \times (\text{PT}(\boldsymbol{\beta})f[4, 8, 7, 6]) && (\text{PT}(\boldsymbol{\alpha})f[5, 6, 8, 1]) \times (\text{PT}(\boldsymbol{\beta})f[4, 8, 7, 6]f[5, 1, 2, 3]) \\
& (\text{PT}(\boldsymbol{\alpha})f[8, 1, 2, 3]) \times (\text{PT}(\boldsymbol{\beta})f[4, 8, 7, 6]f[4, 8, 6, 5]) && (\text{PT}(\boldsymbol{\alpha})) \times (\text{PT}(\boldsymbol{\beta})f[4, 8, 7, 6]f[4, 8, 6, 5]f[5, 1, 2, 3])
\end{aligned}$$

indeed evaluate to $\frac{1}{s_{1234}} \left(\frac{1}{s_{12}s_{34}} + \frac{1}{s_{12}s_{123}} \right) \times \frac{1}{s_{78}s_{678}}$. So we have extracted all terms with poles $\frac{1}{s_{12}} \frac{1}{s_{78}} \frac{1}{s_{678}}$ from the result (5.29).

As another illustration, let us apply the above discussion to six point CHY-integrands with $\text{PT}(\boldsymbol{\alpha}) = \langle 123456 \rangle$ fixed, such that we can examine relations between the independent $\text{PT}(\boldsymbol{\beta})$'s. Starting from the identity PT-factor $\text{PT}(\boldsymbol{\beta}) = \langle 123456 \rangle$, we can choose the selecting factors to corresponds to the independent Mandelstam variables $\{s_{12}, s_{23}, s_{34}, s_{45}, s_{56}, s_{61}\}$ and $\{s_{123}, s_{234}, s_{345}\}$. Explicitly, we have

$$\langle 123456 \rangle \times \begin{cases} f^{\text{select}}[6, 1, 2, 3]_{s_{12}} \rightarrow \langle 126543 \rangle \\ f^{\text{select}}[1, 2, 3, 4]_{s_{23}} \rightarrow \langle 132456 \rangle \\ f^{\text{select}}[2, 3, 4, 5]_{s_{34}} \rightarrow \langle 124356 \rangle \\ f^{\text{select}}[3, 4, 5, 6]_{s_{45}} \rightarrow \langle 123546 \rangle \\ f^{\text{select}}[4, 5, 6, 1]_{s_{56}} \rightarrow \langle 123465 \rangle \\ f^{\text{select}}[5, 6, 1, 2]_{s_{61}} \rightarrow \langle 154326 \rangle \end{cases}, \quad \langle 123456 \rangle \times \begin{cases} f^{\text{select}}[6, 1, 3, 4]_{s_{123}} \rightarrow \langle 123654 \rangle \\ f^{\text{select}}[1, 2, 4, 5]_{s_{234}} \rightarrow \langle 143256 \rangle \\ f^{\text{select}}[2, 3, 5, 6]_{s_{345}} \rightarrow \langle 125436 \rangle \end{cases}, \quad (5.32)$$

where the subscripts are to remind which pole we are picking up. The left column shows the results of picking up the terms with a common two-particle pole $\frac{1}{s_{i,i+1}}$, while the right column shows the results of picking up terms with a common three-particle pole $\frac{1}{s_{i,i+1,i+2}}$. It can be simply checked that the six resulting PT-factors in the left column are those evaluating to five diagrams, while the three in the right column are those evaluating to four diagrams, as presented in §3.3.

Based on above results, we can further consider multiplying one more selecting factor. For example, let us take the resulting PT-factor $\langle 123465 \rangle$ from the left column and $\langle 123654 \rangle$ from the right column. For $\langle 123465 \rangle$, it has overall pole $\frac{1}{s_{56}}$ in the evaluated result. From compatibility condition, the selecting factors we can take are those corresponding to poles $\frac{1}{s_{12}}, \frac{1}{s_{23}}, \frac{1}{s_{34}}, \frac{1}{s_{123}}$ and $\frac{1}{s_{234}}$. For $\langle 123654 \rangle$, it has overall pole $\frac{1}{s_{123}}$ in the evaluated result, and from compatibility condition the selecting factors we can take are those

corresponding to poles $\frac{1}{s_{12}}, \frac{1}{s_{23}}, \frac{1}{s_{45}}$ and $\frac{1}{s_{56}}$. Explicitly, we have

$$\langle 123465 \rangle \times \begin{cases} f^{\text{select}}[5, 1, 2, 3]_{s_{12}} \rightarrow \langle 125643 \rangle \\ f^{\text{select}}[1, 2, 3, 4]_{s_{23}} \rightarrow \langle 132465 \rangle \\ f^{\text{select}}[2, 3, 4, 6]_{s_{34}} \rightarrow \langle 124365 \rangle \\ f^{\text{select}}[5, 1, 3, 4]_{s_{123}} \rightarrow \langle 123564 \rangle \\ f^{\text{select}}[1, 2, 4, 6]_{s_{234}} \rightarrow \langle 143265 \rangle \end{cases}, \quad \langle 123654 \rangle \times \begin{cases} f^{\text{select}}[4, 1, 2, 3]_{s_{12}} \rightarrow \langle 124563 \rangle \\ f^{\text{select}}[1, 2, 3, 6]_{s_{23}} \rightarrow \langle 132654 \rangle \\ f^{\text{select}}[6, 5, 4, 1]_{s_{45}} \rightarrow \langle 123645 \rangle \\ f^{\text{select}}[3, 6, 5, 4]_{s_{56}} \rightarrow \langle 123564 \rangle \end{cases}. \quad (5.33)$$

It can be checked that all the resulting PT-factors evaluate to two Feynman diagrams. In fact, all the six resulting PT-factors in the left column of (5.32) can be treated in the same manner as $\langle 123465 \rangle$, which lead to $6 \times 5 = 30$ PT-factors. All the three resulting PT-factors in the right column of (5.32) can be treated in the same manner as $\langle 123654 \rangle$, which in all produce $3 \times 4 = 12$ PT-factors. However, we have over-counted each PT-factor by one since the result is independent of the order of picking up poles. Therefore, the independent PT-factors that can be produced from all resulting PT-factors in (5.32) by multiplying another selecting factor should be $\frac{6 \times 5 + 3 \times 4}{2!} = 21$, which is exactly the number of independent PT-factors that evaluated to two Feynman diagrams.¹⁰ Indeed, it can be checked that the 21 resulting PT-factors as partly shown in (5.33), together with the other not written down, are just those evaluated to two diagrams as presented in §3.3.

Again, based on above result, we can multiply one more selecting factor that is compatible with the previous two. The resulting PT-factors from (5.33) can be shown as

$$\begin{aligned} \langle 125643 \rangle \times \begin{cases} f^{\text{select}}[6, 4, 3, 1]_{s_{34}} \rightarrow \langle 125634 \rangle \\ f^{\text{select}}[4, 3, 2, 5]_{s_{123}} \rightarrow \langle 124653 \rangle \end{cases} & \quad \langle 124563 \rangle \times \begin{cases} f^{\text{select}}[2, 4, 5, 6]_{s_{45}} \rightarrow \langle 125463 \rangle \\ f^{\text{select}}[4, 5, 6, 3]_{s_{56}} \rightarrow \langle 124653 \rangle \end{cases} \\ \langle 132465 \rangle \times \begin{cases} f^{\text{select}}[5, 1, 2, 4]_{s_{123}} \rightarrow \langle 132564 \rangle \\ f^{\text{select}}[1, 3, 4, 6]_{s_{234}} \rightarrow \langle 142365 \rangle \end{cases} & \quad \langle 132654 \rangle \times \begin{cases} f^{\text{select}}[6, 5, 4, 1]_{s_{45}} \rightarrow \langle 132645 \rangle \\ f^{\text{select}}[2, 6, 5, 4]_{s_{56}} \rightarrow \langle 132564 \rangle \end{cases} \\ \langle 124365 \rangle \times \begin{cases} f^{\text{select}}[5, 1, 2, 4]_{s_{12}} \rightarrow \langle 125634 \rangle \\ f^{\text{select}}[1, 2, 3, 6]_{s_{234}} \rightarrow \langle 134265 \rangle \end{cases} & \quad \langle 123645 \rangle \times \begin{cases} f^{\text{select}}[5, 1, 2, 3]_{s_{12}} \rightarrow \langle 125463 \rangle \\ f^{\text{select}}[1, 2, 3, 6]_{s_{23}} \rightarrow \langle 132645 \rangle \end{cases} \\ \langle 123564 \rangle \times \begin{cases} f^{\text{select}}[4, 1, 2, 3]_{s_{12}} \rightarrow \langle 124653 \rangle \\ f^{\text{select}}[1, 2, 3, 5]_{s_{23}} \rightarrow \langle 132564 \rangle \end{cases} & \quad \langle 123564 \rangle \times \begin{cases} f^{\text{select}}[4, 1, 2, 3]_{s_{12}} \rightarrow \langle 124653 \rangle \\ f^{\text{select}}[1, 2, 3, 5]_{s_{23}} \rightarrow \langle 132564 \rangle \end{cases} \\ \langle 143265 \rangle \times \begin{cases} f^{\text{select}}[4, 3, 2, 6]_{s_{23}} \rightarrow \langle 142365 \rangle \\ f^{\text{select}}[1, 4, 3, 2]_{s_{34}} \rightarrow \langle 134265 \rangle \end{cases} & \end{aligned} \quad (5.34)$$

We notice that each PT-factor in (5.33) has two compatible selecting factors, leading to two new PT-factors, all of which evaluate to one Feynman diagram. Since from (5.32) to (5.33), we get 42 PT-factors (of which 21 are independent), in this step we will get $42 \times 2 = 84$ PT-factors. After excluding the double counting, we get $\frac{42 \times 2}{3!} = 14$ independent PT-factors, which are exactly the PT-factors that evaluated to one Feynman diagram. Our results (5.34), together with those not written down, agree with the 14 independent PT-factors that evaluated to one Feynman diagram as presented in §3.3, after deleting the double counting.

¹⁰Alternatively, we can pick up the two poles from $\langle 123456 \rangle$ at the same time, similar to our example (5.31). The resultant integrands will be different at the first glance, but still evaluate to the same amplitudes.

Since now every pole is overall, if we multiply another selecting factor, we will either get an irrelevant result or return to the mother amplitude.

Before closing, we give a criterion on whether a pole s_A is overall with fixed $\text{PT}(\boldsymbol{\alpha})$. First, s_A is a physical pole *iff* A is consecutive with both $\text{PT}(\boldsymbol{\alpha})$ and $\text{PT}(\boldsymbol{\beta})$. Next, we define $\{\overline{A}_{-1}, A_1, A_{-1}, \overline{A}_1\}$ according to $\text{PT}(\boldsymbol{\beta})$, and put $\text{PT}(\boldsymbol{\alpha})$ into the unique form $\text{PT}(\boldsymbol{\alpha}) = \langle A_1 \dots A_{-1} \dots \rangle$. Then s_A is an overall pole *iff* in $\text{PT}(\boldsymbol{\alpha})$ we have $A_{-1} \prec \overline{A}_{-1} \prec \overline{A}_1$, namely, \overline{A}_{-1} precedes \overline{A}_1 . Otherwise, s_A is not an overall pole. This can be easily understood by the zig-zag path in n -gon. Since an overall pole corresponds to a partial triangulation line in the n -gon, a reverse of ordering must happen when the zig-zag path cross this triangulation line.

6 Conclusion

The CHY-integrand of bi-adjoint cubic scalar theory consists of two PT-factors as $\text{PT}(\boldsymbol{\alpha}) \times \text{PT}(\boldsymbol{\beta})$. Once we fix the color ordering of first PT-factor $\text{PT}(\boldsymbol{\alpha})$ as the natural ordering $\mathbf{e} = \langle 12 \dots n \rangle$, the second PT-factor $\text{PT}(\boldsymbol{\beta})$ then can be interpreted as a permutation acting on the identity element. It is shown in this paper that, the pole structure and vertex information of Feynman diagrams evaluated by a CHY-integrand is completely encoded in the permutations of corresponding PT-factors. The cycle representation of permutation, which neatly organizes the external legs into disjoint cycles, manifests the pole and vertex information. More concretely, since a PT-factor is invariant under cyclic rotations and gains at most a sign $(-)^n$ under reversing of color ordering, we are actually considering $2n$ equivalent permutations of a PT-factor. We then write all the equivalent permutations of $\text{PT}(\boldsymbol{\beta})$ into the cycle representation, and pick out the good ones. Those that can be separated to at least three consecutive parts with respect of $\text{PT}(\boldsymbol{\alpha})$ are called V-type cycle representations. Those that can only be separated into two parts, while each part contains more than two elements, are called P-type cycle representations. We show that the CHY-integrand $\text{PT}(\mathbf{e}) \times \text{PT}(\boldsymbol{\beta})$ gives nonzero contributions if and only if the ways of planar separations allowed by all the V-type representations satisfy the constraint (3.44). The Feynman diagram of a CHY-integrand can be completely determined by one V-type cycle representation by going into its substructures, or collectively determined by all P-type cycle representations of a PT-factor. The vertex structure can be obviously seen from the planar separation of V-type or P-type cycle representations. We presented the algorithm to read out the physical poles and vertices from them.

On the other hand, given an effective Feynman diagram, with possible effective higher point vertices, we have proposed a recursive algorithm to obtain directly the correct cycle representation of corresponding PT-factor $\text{PT}(\boldsymbol{\beta})$. We show that cycle representations of any Feynman diagram allow a factorization as Eq. (4.10) with respect to an arbitrary m -point vertex, called a planar splitting. We have figured out that, the cycle representations of subdiagrams that used in the factorization (4.10) are the non-planar splitting ones in the equivalent class of PT-factors of subdiagrams. The same algorithm applies to the subdiagrams as well, so we can reconstruct the cycle representation of any n -point PT-factor basically from three point

PT-factor. We show that all the discussions are parallel in the Feynman diagram and n -gon diagram, while the latter also takes its role in the associahedron discussion.

It is shown in [31] that different PT-factors are neatly connected in the associahedron picture. In this paper, we also investigate the relations among different PT-factors via the reversing permutation on cycles, which corresponds to adding or removing triangulation line in the n -gon diagrams. The merging and splitting of cycles in a cycle representation mainly select terms with the same poles in a result. From the same thought, we further study the relations among PT-factors via the multiplication of certain cross-ratio factor which we call selecting factor. They all give similar topology about how the PT-factors are connected.

Finally, since the planar diagram possess a natural interpretation as the vertices and boundaries of an associahedron, the structure of good cycle representation introduced in this paper can be used to characterize certain boundaries. We have shown how this can be achieved by merging of cycles, in the equivalent class of a $\text{PT}(\beta)$, the number of different factorizations into disjoint permutations describes the shape of boundaries of the associahedron.

Acknowledgments

We thank Song He for helpful discussions. We also thank the hospitality of the Institute of Theoretical Physics at Chinese Academy of Science, where this work was initiated. B.F. is supported by Qiu-Shi Funding and the National Natural Science Foundation of China (NSFC) with Grant No.11575156 and No.11135006. R.H. is supported by the NSFC with Grant No.11575156 and the starting grant from Nanjing Normal University. F.T. is supported in part by the Knut and Alice Wallenberg Foundation under grant KAW 2013.0235 and the Ragnar Söderberg Foundation under grant S1/16.

A Associahedron and cycle representation of permutation

As we have briefly mentioned, all the cubic scalar diagrams are related to the associahedron. More concretely, all the n -point PT-factors can be elegantly encoded into an associahedron denoted as \mathcal{K}_{n-1} , which is an $(n-3)$ -dimensional convex polytope whose vertices are labeled by n -point cubic diagrams. The two vertices connected by an edge represent the two diagrams that share the same $(n-4)$ internal edges, such that we can label the edges with those diagrams with $(n-4)$ cubic vertices and one quartic vertex. In general, an k -dimensional boundary consists of vertices that share the same $(n-3-k)$ internal edges. The number of k -dimensional boundaries in \mathcal{K}_{n-1} is given by the equation¹¹

$$T(n, k) = \binom{k}{n-3} \binom{n-k-3}{2n-k-4} \frac{1}{n-k-2}. \quad (\text{A.1})$$

All these boundaries correspond to diagrams with higher point vertices. They are thus characterized by the vertex number vector

$$\mathbf{v} \equiv (v_3, v_4, v_5, \dots, v_n), \quad (\text{A.2})$$

¹¹See <https://oeis.org/A033282>

where v_i satisfies the constraint of (4.7). For instance, at $n = 6$, the three-dimensional associahedron \mathcal{K}_5 has two kinds of faces (two-dimensional boundaries): pentagon (\mathcal{K}_4) and rectangle ($\mathcal{K}_3 \times \mathcal{K}_3$). They correspond to the diagrams with $\mathbf{v} = (1, 0, 1, 0)$ and $(0, 2, 0, 0)$ respectively. All the boundaries of \mathcal{K}_{n-1} can be obtained by direct products of lower dimensional associahedrons. We use $N_n(v_3, v_4, \dots, v_n)$ to denote the number of boundaries \mathcal{K}_{n-1} that are of the form

$$\underbrace{\mathcal{K}_2 \times \dots \times \mathcal{K}_2}_{v_3} \times \underbrace{\mathcal{K}_3 \times \dots \times \mathcal{K}_3}_{v_4} \times \underbrace{\mathcal{K}_4 \times \dots \times \mathcal{K}_4}_{v_5} \times \dots . \quad (\text{A.3})$$

In particular, $N_n(n-2, 0, \dots, 0)$ gives the number of vertices of \mathcal{K}_{n-1} , which is the Catalan number $C_n = \frac{(2n-4)!}{(n-1)!(n-2)!}$, and $N_n(0, 0, \dots, 0, 1) = 1$ just stands for the \mathcal{K}_{n-1} itself.

Knowing the relation between cycle representations and Feynman diagrams, we can give the number $N_n(v_3, v_4, \dots, v_n)$ another interpretation. From §4.2, we know that a PT-factor $\text{PT}(\boldsymbol{\beta})$ corresponds to a Feynman diagram with $\mathbf{v} = (v_3, v_4 \dots v_n)$ only if among the $(2n)$ elements of its equivalent class, there are exactly v_i different cycle partitions $\{\boldsymbol{\beta}_{A_1}^{\text{cyc-rep}}, \dots, \boldsymbol{\beta}_{A_i}^{\text{cyc-rep}}\}$ such that

$$\boldsymbol{\beta}_{A_1}^{\text{cyc-rep}} \boldsymbol{\beta}_{A_2}^{\text{cyc-rep}} \dots \boldsymbol{\beta}_{A_i}^{\text{cyc-rep}} \in \mathfrak{b}[\boldsymbol{\beta}] \quad , \quad 3 \leq i \leq n ,$$

where each $\boldsymbol{\beta}_{A_i}^{\text{cyc-rep}}$ can not be further split planarly. Then the number $N_n(\mathbf{v})$ simply counts the number of such permutations. To clarify this statement, a few typical examples are in order. First, at $n = 6$, the PT-factor $\langle 123465 \rangle$ corresponds to a diagram with two quartic vertices, namely, $\mathbf{v} = (0, 2, 0, 0)$,

$$\begin{array}{c} 3 \quad 4 \\ | \quad | \\ 2 \text{---} \text{---} 5 \\ | \quad | \\ 1 \quad 6 \end{array} \iff \text{PT}(\boldsymbol{\beta}) = \langle 123465 \rangle . \quad (\text{A.4})$$

In the equivalent class of $\langle 123465 \rangle$, there are two cycle representations that can be split planarly, and there are in all two ways to split them into four planar parts,

$$\begin{aligned} (1)|(2)|(3)|(46)(5) &\implies \boldsymbol{\beta}_{A_1}^{\text{cyc-rep}} = (1) \quad , \quad \boldsymbol{\beta}_{A_2}^{\text{cyc-rep}} = (2) \quad , \quad \boldsymbol{\beta}_{A_3}^{\text{cyc-rep}} = (3) \quad , \quad \boldsymbol{\beta}_{A_4}^{\text{cyc-rep}} = (46)(5) \\ (13)(2)|(4)|(5)|(6) &\implies \boldsymbol{\beta}_{A_1}^{\text{cyc-rep}} = (13)(2) \quad , \quad \boldsymbol{\beta}_{A_2}^{\text{cyc-rep}} = (4) \quad , \quad \boldsymbol{\beta}_{A_3}^{\text{cyc-rep}} = (5) \quad , \quad \boldsymbol{\beta}_{A_4}^{\text{cyc-rep}} = (6) \end{aligned} . \quad (\text{A.5})$$

Now comparing with Eq. (A.5), we see that the two four-part planar splitting is due to the fact that the corresponding Feynman diagram consist of two quartic vertices. Since each subdiagram can also be factorized to sub-subdiagrams, this allows a recursive computation for $N_n(\mathbf{v})$, down to the pieces where only cubic vertices exist and only length-1 or length-2 cycles appear in the cycle representation. Thus $\langle 123465 \rangle$ contributes to the counting $N_6(0, 2, 0, 0)$. Next, we consider an eight point example with $\mathbf{v} = (2, 2, 0, 0, 0, 0)$,

$$\begin{array}{c} 3 \quad 4 \\ | \quad | \\ 2 \text{---} \text{---} 5 \\ | \quad | \\ 1 \quad 6 \\ | \quad | \\ 8 \quad 7 \end{array} \iff \text{PT}(\boldsymbol{\beta}) = \langle 12846573 \rangle . \quad (\text{A.6})$$

In the equivalent class of $\langle 12846573 \rangle$, there are again two cycle representations that have planar splittings, but this time there are two ways to split them into three parts (blue partitions), and two ways to split them into four parts (red partitions),

$$(1)|(2)|(38)|(4)|(56)|(7) \quad , \quad (8)|(12)|(3)|(47)|(5)|(6) . \quad (\text{A.7})$$

Again, the cycle splitting pattern agrees exactly with the vertex number vector $(2, 2, 0, 0, 0, 0)$. Thus the PT-factor $\langle 12846573 \rangle$ contributes to the counting $N_8(2, 2, 0, 0, 0, 0)$. The above machinery can also be used to pick out those PT-factors that do not give any Feynman diagram. We again illustrate this point by a few examples first. At $n = 6$, we consider the PT-factor $\langle 124635 \rangle$. In its equivalent class, there is only one three-part cycle partition,

$$(1)|(2)|(3465) . \quad (\text{A.8})$$

Had this PT-factor given any Feynman diagram, the vertex number vector would be $\mathbf{v} = (1, 0, 0, 0)$. Since this \mathbf{v} does not satisfy the constraint (4.7), $\langle 124635 \rangle$ does not correspond to any Feynman diagram compatible with the planar order $\langle 123456 \rangle$. Similarly, the PT-factor $\langle 135264 \rangle$ does not have any valid cycle partition (namely, more than three parts) in its equivalent class, it must also give zero Feynman diagram. In general, by inspecting how the cycle representations of a PT-factor split, we can get a vertex number vector \mathbf{v} . If this \mathbf{v} fails to satisfy the constraint (4.7), the PT-factor under consideration must give zero Feynman diagram.

In order to write down a recursive formula for N_n , let us consider the following factorization of Feynman diagram. Starting from an arbitrary external leg, it would connect to, say, a $(s + 1)$ -point vertex. This vertex splits the diagram into $(s + 1)$ subdiagrams. One of the subdiagram is just the single external leg we started from, which does not contain any other external legs of the Feynman diagram. The remaining $(n - 1)$ external legs are separated into the other s subdiagrams. Let us assume that the number of legs is x_i for each subdiagram i , with $1 \leq i \leq s$. Since each subdiagram consists of external legs and an internal propagator, we would have the following constraint

$$\sum_{i=1}^s x_i = (n - 1) + s . \quad (\text{A.9})$$

If the vertex number vector for each subdiagram is \mathbf{u}_i , then we have the following constraint

$$\sum_{i=1}^s \mathbf{u}_i = (v_3, v_4, \dots, v_s, v_{s+1} - 1, v_{s+2}, \dots, v_n) , \quad (\text{A.10})$$

where $\mathbf{v} = (v_3, v_4, \dots, v_n)$ is the vertex number vector of the complete Feynman diagram, and v_m is the number of the m -point vertices. The meaning of Eq. (A.10) is clear: summing over the numbers of m -point vertices in all the subdiagrams should give the number of m -point vertices in the complete Feynman diagram, except that the number of $(s + 1)$ -point vertex should be reduced by one, since the $(s + 1)$ -point

$n = 6$					$n = 8$				
\mathbf{v}	F	$N_n(\mathbf{v})$	$T(n, k)$	k	\mathbf{v}	F	$N_n(\mathbf{v})$	$T(n, k)$	k
(4, 0, 0, 0)	1	14	14	0	(6, 0, 0, 0, 0, 0)	1	132	132	0
(2, 1, 0, 0)	2	21	21	1	(4, 1, 0, 0, 0, 0)	2	330	330	1
(1, 0, 1, 0)	5	6	9	2	(3, 0, 1, 0, 0, 0)	5	120	300	2
(0, 2, 0, 0)	4	3			(2, 2, 0, 0, 0, 0)	4	180		
(0, 0, 0, 1)	14	1	1	3	(2, 0, 0, 1, 0, 0)	14	36	120	3
$n = 7$					(1, 1, 1, 0, 0, 0)	10	72		
\mathbf{v}	F	$N_n(\mathbf{v})$	$T(n, k)$	k	(0, 3, 0, 0, 0, 0)	8	12	20	4
(5, 0, 0, 0, 0)	1	42	42	0	(1, 0, 0, 0, 1, 0)	42	8		
(3, 1, 0, 0, 0)	2	84	84	1	(0, 2, 0, 1, 0, 0)	28	8	1	5
(2, 0, 1, 0, 0)	5	28	56	2	(0, 0, 2, 0, 0, 0)	25	4		
(1, 2, 0, 0, 0)	4	28			(0, 0, 0, 0, 0, 1)	132	1	1	
(1, 0, 0, 1, 0)	14	7	14	3					
(0, 1, 1, 0, 0)	10	7							
(0, 0, 0, 0, 1)	42	1	1	4					

Table 1: $N_n(\mathbf{v})$ and the corresponding $T(n, k)$ for $n = 6, 7$ and 8 . In addition, F gives the number of trivalent Feynman diagrams.

vertex that connects the starting external leg has been split and does not belong to any subdiagram¹². Then N_n can be recursively computed from those N_{x_i} 's of the subdiagrams as,

$$N_n(v_3, v_4, \dots, v_n) = \sum_{s=2}^{n-1} \sum_{\{x_i\}} \sum_{\{\mathbf{u}_i\}} N_{x_1}(\mathbf{u}_1) N_{x_2}(\mathbf{u}_2) \cdots N_{x_s}(\mathbf{u}_s), \quad (\text{A.11})$$

where for each $2 \leq s \leq n-2$, the summation over $\{x_i\}$ and $\{\mathbf{u}_i\}$ are constrained respectively by Eq. (A.9) and (A.10), and s takes the value k whenever v_{k+1} is not zero. We note that by definition the vector \mathbf{u}_i satisfies the constraint,

$$\sum_{m=3}^{x_i} (m-2) u_{im} = x_i - 2. \quad (\text{A.12})$$

In addition, we also require that each $x_i \geq 2$ and each component of \mathbf{u}_i is non-negative. The recursion starts at $N_2(0) = 1$. If $\mathbf{v} = (n-2, 0, \dots, 0)$, i.e., all $v_i = 0$ except that $v_3 = n-2$, then s can only take $s = 2$ in (A.11), which gives nothing but the recursion for the Catalan numbers. For low multiplicity, one

¹²The \mathbf{u}_i in (A.10) is the vertex number vector of x_i -point subdiagram, so it has $x_i - 2$ components $\mathbf{u}_i = (u_{i3}, u_{i4}, \dots, u_{ix_i})$. When we equal the left and right side of (A.10), all the u_{ik} with $x_i + 1 \leq k \leq n$ are automatically understood to be zero.

can easily find that,

$$\begin{aligned}
N_3(1) = 1, & & N_4(2, 0) = 2, & & N_5(3, 0, 0) = 5, \\
& & N_4(0, 1) = 1, & & N_5(1, 1, 0) = 5, \\
& & & & N_5(0, 0, 1) = 1.
\end{aligned} \tag{A.13}$$

The cases of $n = 6, 7$ and 8 are shown in Table 1, where we can easily check that the values of $N_6(\mathbf{v})$, for example, agree with the counting of Feynman diagrams. By knowing the values for lower multiplicities, we can easily calculate, for example,

$$\begin{aligned}
N_7(0, 1, 1, 0, 0) &= N_2(0)N_2(0)N_5(0, 0, 1) + N_2(0)N_5(0, 0, 1)N_2(0) + N_5(0, 0, 1)N_2(0)N_2(0) \\
&+ N_2(0)N_2(0)N_2(0)N_4(0, 1) + N_2(0)N_2(0)N_4(0, 1)N_2(0) \\
&+ N_2(0)N_4(0, 1)N_2(0)N_2(0) + N_4(0, 1)N_2(0)N_2(0)N_2(0) \\
&= 7.
\end{aligned} \tag{A.14}$$

The value of N_n , as a complement of $T(n, k)$, further distinguishes different shapes of k -dimensional boundary of associahedron \mathcal{K}_{n-1} .

References

- [1] F. Cachazo, S. He and E. Y. Yuan, *Scattering in Three Dimensions from Rational Maps*, *JHEP* **10** (2013) 141, [[1306.2962](#)].
- [2] F. Cachazo, S. He and E. Y. Yuan, *Scattering equations and Kawai-Lewellen-Tye orthogonality*, *Phys. Rev. D* **90** (2014) 065001, [[1306.6575](#)].
- [3] F. Cachazo, S. He and E. Y. Yuan, *Scattering of Massless Particles in Arbitrary Dimensions*, *Phys.Rev.Lett.* **113** (2014) 171601, [[1307.2199](#)].
- [4] F. Cachazo, S. He and E. Y. Yuan, *Scattering of Massless Particles: Scalars, Gluons and Gravitons*, *JHEP* **1407** (2014) 033, [[1309.0885](#)].
- [5] L. Mason and D. Skinner, *Ambitwistor strings and the scattering equations*, *JHEP* **07** (2014) 048, [[1311.2564](#)].
- [6] Y. Geyer, A. E. Lipstein and L. J. Mason, *Ambitwistor Strings in Four Dimensions*, *Phys. Rev. Lett.* **113** (2014) 081602, [[1404.6219](#)].
- [7] E. Casali and P. Tourkine, *On the null origin of the ambitwistor string*, *JHEP* **11** (2016) 036, [[1606.05636](#)].
- [8] W. Siegel, *Amplitudes for left-handed strings*, [[1512.02569](#)].
- [9] Y. Li and W. Siegel, *Chiral Superstring and CHY Amplitude*, [[1702.07332](#)].
- [10] N. Berkovits, *Infinite Tension Limit of the Pure Spinor Superstring*, *JHEP* **03** (2014) 017, [[1311.4156](#)].
- [11] H. Gomez and E. Y. Yuan, *N -point tree-level scattering amplitude in the new Berkovits' string*, *JHEP* **04** (2014) 046, [[1312.5485](#)].

- [12] N. E. J. Bjerrum-Bohr, P. H. Damgaard, P. Tourkine and P. Vanhove, *Scattering Equations and String Theory Amplitudes*, *Phys. Rev.* **D90** (2014) 106002, [[1403.4553](#)].
- [13] F. Cachazo and H. Gomez, *Computation of Contour Integrals on $\mathcal{M}_{0,n}$* , *JHEP* **04** (2016) 108, [[1505.03571](#)].
- [14] C. Baadsgaard, N. E. J. Bjerrum-Bohr, J. L. Bourjaily and P. H. Damgaard, *Integration Rules for Scattering Equations*, *JHEP* **09** (2015) 129, [[1506.06137](#)].
- [15] C. Baadsgaard, N. E. J. Bjerrum-Bohr, J. L. Bourjaily and P. H. Damgaard, *Scattering Equations and Feynman Diagrams*, *JHEP* **09** (2015) 136, [[1507.00997](#)].
- [16] C. Baadsgaard, N. E. J. Bjerrum-Bohr, J. L. Bourjaily, P. H. Damgaard and B. Feng, *Integration Rules for Loop Scattering Equations*, *JHEP* **11** (2015) 080, [[1508.03627](#)].
- [17] C. S. Lam and Y.-P. Yao, *Evaluation of the Cachazo-He-Yuan gauge amplitude*, *Phys. Rev.* **D93** (2016) 105008, [[1602.06419](#)].
- [18] R. Huang, B. Feng, M.-x. Luo and C.-J. Zhu, *Feynman Rules of Higher-order Poles in CHY Construction*, *JHEP* **06** (2016) 013, [[1604.07314](#)].
- [19] C. Cardona, B. Feng, H. Gomez and R. Huang, *Cross-ratio Identities and Higher-order Poles of CHY-integrand*, *JHEP* **09** (2016) 133, [[1606.00670](#)].
- [20] N. E. J. Bjerrum-Bohr, J. L. Bourjaily, P. H. Damgaard and B. Feng, *Manifesting Color-Kinematics Duality in the Scattering Equation Formalism*, *JHEP* **09** (2016) 094, [[1608.00006](#)].
- [21] R. Huang, Y.-J. Du and B. Feng, *Understanding the Cancellation of Double Poles in the Pfaffian of CHY-formalism*, *JHEP* **06** (2017) 133, [[1702.05840](#)].
- [22] K. Zhou, J. Rao and B. Feng, *Derivation of Feynman Rules for Higher Order Poles Using Cross-ratio Identities in CHY Construction*, *JHEP* **06** (2017) 091, [[1705.04783](#)].
- [23] S. Stieberger and T. R. Taylor, *New relations for Einstein-Yang-Mills amplitudes*, *Nucl. Phys.* **B913** (2016) 151–162, [[1606.09616](#)].
- [24] D. Nandan, J. Plefka, O. Schlotterer and C. Wen, *Einstein-Yang-Mills from pure Yang-Mills amplitudes*, *JHEP* **10** (2016) 070, [[1607.05701](#)].
- [25] C.-H. Fu, Y.-J. Du, R. Huang and B. Feng, *Expansion of Einstein-Yang-Mills Amplitude*, *JHEP* **09** (2017) 021, [[1702.08158](#)].
- [26] F. Teng and B. Feng, *Expanding Einstein-Yang-Mills by Yang-Mills in CHY frame*, *JHEP* **05** (2017) 075, [[1703.01269](#)].
- [27] Y.-J. Du and F. Teng, *BCJ numerators from reduced Pfaffian*, *JHEP* **04** (2017) 033, [[1703.05717](#)].
- [28] Y.-J. Du, B. Feng and F. Teng, *Expansion of All Multitrace Tree Level EYM Amplitudes*, *JHEP* **12** (2017) 038, [[1708.04514](#)].
- [29] Z. Bern, J. J. M. Carrasco and H. Johansson, *New relations for gauge-theory amplitudes*, *Phys. Rev. D* **78** (2008) 085011, [[0805.3993](#)].
- [30] Z. Bern, J. J. M. Carrasco and H. Johansson, *Perturbative Quantum Gravity as a Double Copy of Gauge Theory*, *Phys. Rev. Lett.* **105** (2010) 061602, [[1004.0476](#)].

- [31] N. Arkani-Hamed, Y. Bai, S. He and G. Yan, *Scattering Forms and the Positive Geometry of Kinematics, Color and the Worldsheet*, [1711.09102](#).
- [32] C. S. Lam and Y.-P. Yao, *Role of Möbius constants and scattering functions in Cachazo-He-Yuan scalar amplitudes*, *Phys. Rev.* **D93** (2016) 105004, [[1512.05387](#)].
- [33] X. Gao, S. He and Y. Zhang, *Labelled tree graphs, Feynman diagrams and disk integrals*, *JHEP* **11** (2017) 144, [[1708.08701](#)].
- [34] L. de la Cruz, A. Kniss and S. Weinzierl, *Properties of scattering forms and their relation to associahedra*, [1711.07942](#).
- [35] R. Kenyon and J.-M. Schlenker, *Rhombic embeddings of planar graphs with faces of degree 4*, *ArXiv Mathematical Physics e-prints* (May, 2003) , [[math-ph/0305057](#)].
- [36] A. Hanany and D. Vegh, *Quivers, tilings, branes and rhombi*, *JHEP* **10** (2007) 029, [[hep-th/0511063](#)].
- [37] B. Feng, Y.-H. He, K. D. Kennaway and C. Vafa, *Dimer models from mirror symmetry and quivering amoebae*, *Adv. Theor. Math. Phys.* **12** (2008) 489–545, [[hep-th/0511287](#)].
- [38] B. Feng, *CHY-construction of Planar Loop Integrands of Cubic Scalar Theory*, *JHEP* **05** (2016) 061, [[1601.05864](#)].